# Underground Coal Thermal Treatment

Task 6 Topical Report, Utah Clean Coal Program

Reporting Period Start Date: April 2012

Report Period End Date: August 2014

Principal Authors: P.J. Smith, M. Deo, E.G. Eddings, M. Hradisky, K.E. Kelly, R. Krumm, Adel F. Sarofim, D. Wang

Issue date: January 2015

DOE Award Number: DE-NT0005015
Project Officer: David Lang

University of Utah
Institute for Clean & Secure Energy
380 INSCC
155 South, 1452 East
Salt Lake City, UT 84112

**DISCLAIMER**

**ABSTRACT**

The long-term objective of this task is to develop a transformational energy production technology by in-situ thermal treatment of a coal seam for the production of substitute natural gas and/or liquid transportation fuels while leaving much of the coal's carbon in the ground. This process converts coal to a high-efficiency, low-greenhouse gas (GHG) emitting fuel. It holds the potential of providing environmentally acceptable access to previously unusable coal resources. This task focused on three areas:

- *Experimental*. The Underground Coal Thermal Treatment (UCTT) team focused on experiments at two scales, bench-top and slightly larger, to develop data to understand the feasibility of a UCTT process as well as to develop validation/uncertainty quantification (V/UQ) data for the simulation team.

- *Simulation*. The investigators completed development of High Performance Computing (HPC) simulations of UCTT. This built on our simulation developments over the course of the task and included the application of Computational Fluid Dynamics (CFD)- based tools to perform HPC simulations of a realistically sized domain representative of an actual coal field located in Utah.

- *$CO_2$ storage*. In order to help determine the amount of $CO_2$ that can be sequestered in a coal formation that has undergone UCTT, adsorption isotherms were performed on coals treated to 325, 450, and 600°C with slow heating rates. Raw material was sourced from the Sufco (Utah), Carlinville (Illinois), and North Antelope (Wyoming) mines. The study indicated that adsorptive capacity for the coals increased with treatment temperature and that coals treated to 325°C showed less or similar capacity to the untreated coals.

**TABLE OF CONTENTS**

**LIST OF FIGURES**

**LIST OF TABLES**

**LIST OF ABBREVIATIONS**

| | |
|---|---|
| BET | Brunauer-Emmett-Teller |
| BJH | Barrett-Joyner-Halenda |
| CFD | Computational fluid dynamics |
| DAF | Dry ash free |
| DEM | Discrete element method |
| DFT | Density functional theory |
| FBR | Fixed-bed reactor |
| GHG | Greenhouse gas |
| HPC | High-performance computing |
| HHV | Higher heating value |
| NER | Net energy return |
| PSD | Pore size distribution |
| RBR | Rubblized-bed reactor |
| SCN | Single carbon number |
| UCTT | Underground coal thermal treatment |
| V/UQ | Validation/uncertainty quantification |

## EXECUTIVE SUMMARY

The long-term objective of this task is to develop a transformational energy production technology by in-situ thermal treatment of a coal seam for the production of substitute natural gas and/or liquid transportation fuels while leaving much of the coal's carbon in the ground. In this process the coal seam is heated indirectly with some thermal source to produce light gases and tars, as opposed to traditional underground coal gasification where the combustion and gasification reactions provide the heat for pyrolysis. Subsequently, the heated formation will be used to inject $CO_2$ captured from other surface processes and thus serve as a $CO_2$ storage reservoir for sequestration. This process converts coal to a high-efficiency, low-GHG emitting fuel. It holds the potential of providing environmentally acceptable access to previously unusable coal resources. By increasing the abundance of cleaner fuels from coal, the proposed technology has the potential for significantly lowering fuel prices relative to other energy sources, and reducing the carbon footprint of coal utilization, thus providing the economic and environmental drivers for displacing imported energy sources.

The task included three interconnected components, experimental, simulation and carbon dioxide storage. All of the work focused on high-volatile subbituminous Utah coal, either Sufco or Skyline, depending on the availability.

*Experimental.* The UCTT experimental work entailed developing reactors at two scales, the ¾" diameter, 6" long, fixed-bed reactor (FBR) and the 6" diameter, 36" long, rubblized-bed reactor (RBR). The goal of the scoping studies was to begin to identify conditions, which would maximize yield and narrow the number of difficult RBR experiments that needed to be run. Both experiments provided relatively consistent results where the yield appeared to be highly dependent on final temperature, with pressure being a secondary factor. A mass balance performed on the RBR products indicated that carbon partitioned preferentially to the char, and hydrogen partitioned preferentially to the gas and liquid products.

*Simulation.* The investigators completed HPC simulations of UCTT using a realistic coal properties, based on the experimental studies, and realistically sized domain representative of an actual coal field located in Utah. These studies focused on the investigation of heat transfer and yield models, as well as various seam thicknesses and heater temperatures. These studies suggested the importance of developing an accurate yield model for the low temperatures. Although numerous yield models exist, these are designed for the high temperatures and high heating rates associated with pulverized coal combustion, not the low temperatures present in a UCTT process.

*Carbon dioxide storage.* The UCTT sequestration work focused on adsorption of $CO_2$ in Utah Sufco bituminous, Illinois Carlinville bituminous, and Wyoming North Antelope subbituminous coals that were pyrolized to final temperatures of 325, 450, or 600°C with heating rates of either 10 or 0.1°C/minute. Adsorption isotherms and pore size studies were performed on the pryolized and unpryrolized coals. Pore size distributions helped explain the connection between adsorptive capacity and terminal treatment temperature. Adsorption isotherms were measured volumetrically at 50 and 70°C using either $CO_2$ or $CH_4$ as the adsorptive.

The results of the adsorption studies of $CH_4$ and $CO_2$ on the thermally treated coals increased with treatment temperature. As expected, the capacity for $CO_2$ was greater than that of methane; also, the capacity was higher when measured at 50°C than when measured at 70°C. Coals that were treated to 325°C showed less or similar adsorptive capacity to unreacted coals. Little influence of heating rate was seen with the high-pressure adsorption measurements. These trends occurred for all coals in this study. Pore size studies found that a fraction of the surface area and micro- and mesopores are attributable to residual tars. Preliminary measurements found similar trends between pore size distributions and adsorptive capacity. Since small pores often serve as sites for capillary condensation, using pore size distributions to relate thermal treatment conditions to adsorptive capacity is a logical approach. A good correlation was developed between the abundance of mesopores (2-50nm) and adsorptive capacity.

## INTRODUCTION

With current coal mining technologies and production rates, approximately 240 years of coal reserves are domestically available (BP 2012). In addition to recoverable coal reserves, the US has vast coal resources, which are unrecoverable due to their depth, access, and other factors (US EIA 2012a; Figure 1). These current recoverable and unrecoverable coal resources provide an opportunity for an in situ technology to recover otherwise unrecoverable energy from coal. Although natural gas prices are at historic lows in the United States, the EIA projects a steady increase in prices, and prices will increase more rapidly when the US begins exporting natural gas (US EIA 2012b).

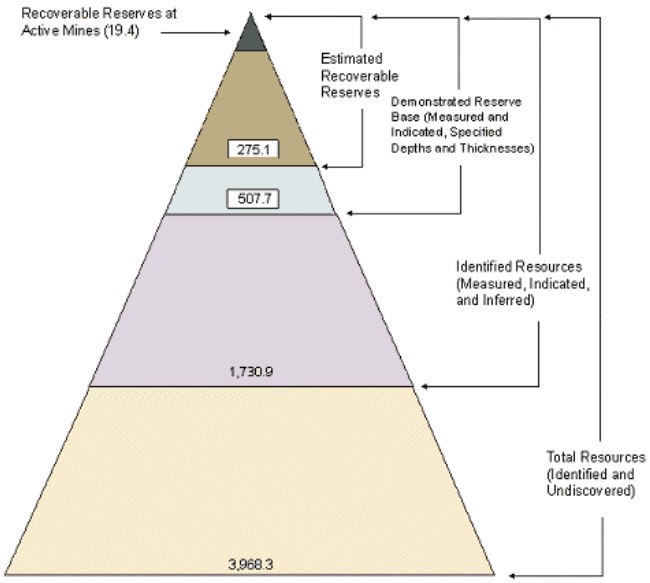


Figure 1. US Coal resources and reserves (1998) in billions of short tons (Clean Energy-US 2012a).

Figure 2 illustrates one example of UCTT including carbon management. UCTT transforms coal in the ground to a synthetic gas stream containing hydrogen, low molecular-weight hydrocarbons and potentially to liquid fuels by slowly heating it. The product flows to a power plant or to a processing facility (if the products are intended for sale). This process has the potential to leave large portions of the

carbon from the coal in the ground. For power generation, GHG gas emissions can further be controlled by capture of $CO_2$ and reinjecting it into the coal seam during and after product recovery, or for use in enhanced oil recovery. Injection of $CO_2$ may also enhance gas production if injected during treatment. Although UCTT requires additional energy input compared to CBM, the added resource utilization and carbon management may be make this process worthwhile and motivates its evaluation.

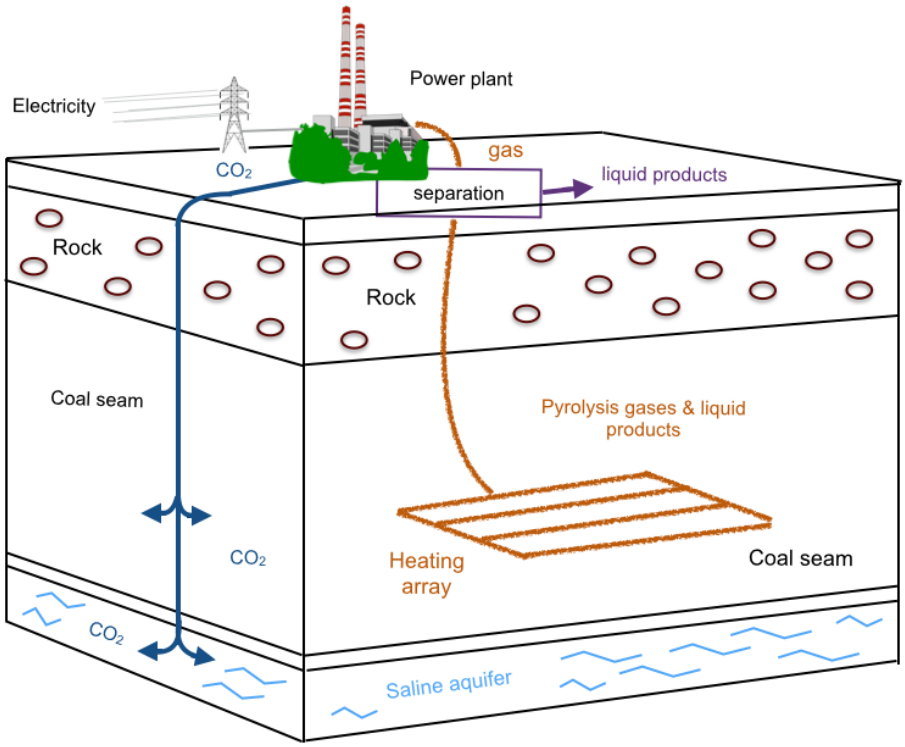


Figure 2. Example of a UCTT process.

## METHODS

### Experimental studies

Both the scoping tests and the RBR experiments were performed with Utah Sufco coal in a nitrogen environment. This high-volatile bituminous coal (38.6% volatile matter, as received) has a relatively low moisture content (3%) and is expected to provide a better volatile yield than some other coals. Table 1 shows the average ultimate and proximate analyses of the coal (before pyrolysis) and char (after pyrolysis) samples. The moisture content was on average 3.2 ± 0.15 % before pyrolysis and 1.31 ± 0.27 % after pyrolysis. The ash content was more variable with an average of 5.04 ± 1.82 % before pyrolysis and 5.32 ± 2.13 % after pyrolysis, which could indicate that inclusions in the coal are affecting the composition. The coal's heating value was 14,078 btu/lb (as received).

Table 1. Ultimate and proximate analyses for the coal (average of 6 samples) and char (average of 11 different samples). The results are in weight percent on a dry ash free basis.

| | Proximate analyses | | Ultimate analyses | | | | |
|---|---|---|---|---|---|---|---|
| | FC | V | C | H | N | O | S |
| Coal | 54.8 ± 0.62 | 45.3 ± 0.62 | 78.5 ± 0.22 | 5.61 ± 0.06 | 1.72 ± 0.06 | 13.6 ± 0.28 | 0.65 ± 0.08 |
| Char | 90.9 ± 3.10 | 9.07 ± 3.10 | 91.8 ± 1.89 | 2.19 ± 0.55 | 2.09 ± 0.17 | 3.34 ± 1.30 | 0.6 2± 0.15 |

FC: fixed carbon; V: volatile content; C: carbon; H: hydrogen; N: nitrogen; O: oxygen; S: sulfur.

**Scoping studies**

Experimental scoping studies used the University of Utah's FBR, which has a ¾" diameter and a 6" bed length (Figure 3). The FBR can be operated at pressures up to 300 psi and temperatures up to 800°C. It can operate under a variety of atmospheres including nitrogen, helium, argon, $CO_2$ and steam. The reactor exit is designed to allow for condensation and collection of tar and liquid products, then to route the gas products to a gas chromatograph for analysis. The goal of these scoping studies is to identify the most promising experimental conditions (i.e., heating rate, final temperature, environment, etc.) for the larger-scale, and more expensive, experiments in the RBR. Table 2 presents the matrix of FBR scoping tests.

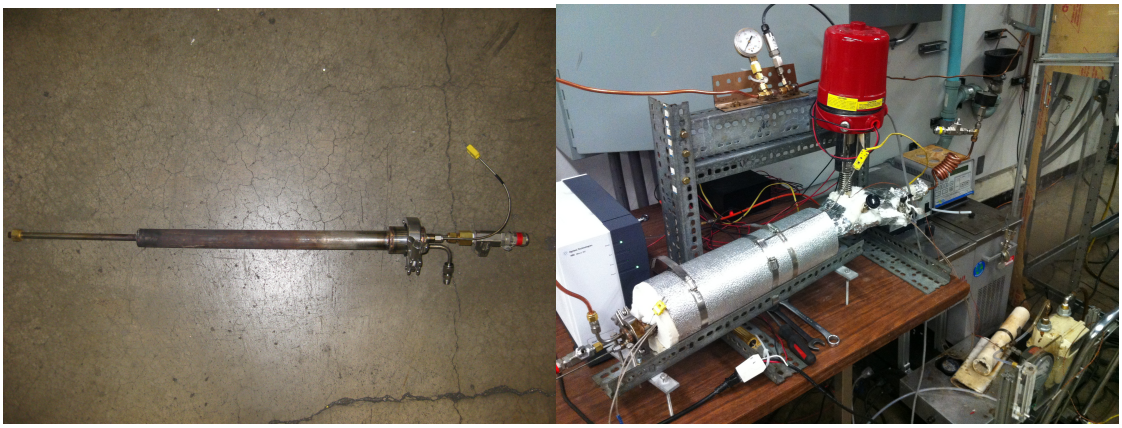

Figure 3. Fixed bed reactor.

Table 2. Experimental test matrix for scoping studies.

| Temperature (°C) | Pressure (atm) | Heating Rate (C/min) |
|---|---|---|
| 400 | 1 | 10 |
| *500* | *1* | *10* |
| 600 | 1 | 1 |
| 400 | 20 | 1 |
| 600 | 20 | 1 |
| *400* | *1* | *10 (replicate)* |
| 600 | 20 | 10 |
| *600* | *20* | *10 (replicate)* |

**RBR studies**

Larger scale studies were performed in the RBR. The RBR is equipped with sampling ports for analysis of product composition. The reactor can operate at pressures up to 1500 psi and temperatures up to 600$^{o}$C. The RBR utilizes a unique two-vessel design to achieve its severe operating thresholds. The outer vessel is an 18" diameter pressure vessel that is built to withstand the maximum operating pressure at temperatures up to 300$^{o}$C. Housed inside the pressure vessel is a 6" diameter vessel that contains the rubblized coal bed. The inner vessel has an electrical heat source that conductively heats adjacent coal blocks and induces convective currents in the free spaces between blocks. An array of thermocouples provides temperature data in various regions of the block (See Appendix A for details). External lines through both vessels permits a steady purge of nitrogen (5.87 l/min) so that gas samples can be collected during pyrolysis.

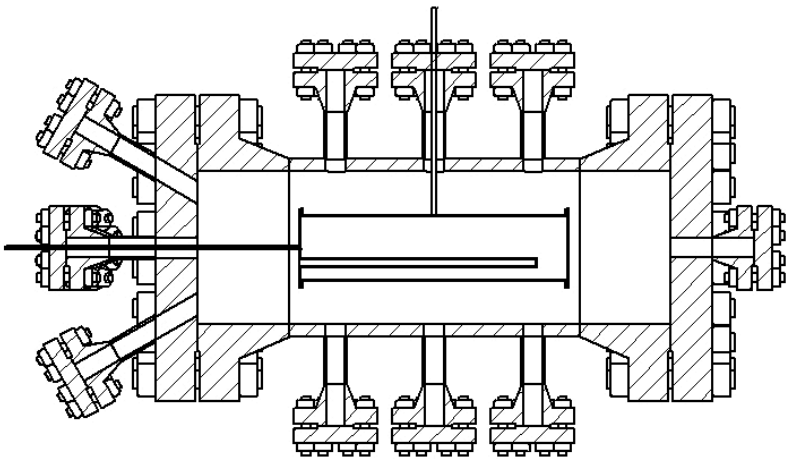

Figure 4. Cross-sectional view of the rubblized-bed reactor.

Based on the scoping studies, selected experiments were performed in the RBR. In addition to providing a more realistic heating profile, the RBR can allow examination of the effect of coal rubblization. Table 3 shows the experimental matrix. Because the high-pressure experiments were so difficult to perform, the team was only able to perform a limited number of these.

Table 3. Summary of completed RBR experiments as well as gas and liquid yields.

| Run # | Date | Pressure (psi) | SS Temp C inside/all[1] | Temp Range (all) °C | Temp STDEV (all) °C | Coal | C7+ liquid yield[2] | Gas yield[2] |
|---|---|---|---|---|---|---|---|---|
| 1 | incomplete | | | | | | | |
| 2 | incomplete | | | | | | | |
| 3 | 2/13/14 | 15 | 520/532 | 426-588 | 58.0 | Chunk | 12% | 16% |
| 4 | 3/10/14 | 15 | 558/562 | 460-621 | 53.7 | Rubble | | |
| 5 | 3/13/14 | 15 | 382/398 | 349-436 | 31.3 | Rubble | 8% | 12% |
| 6 | 3/28/14 | 300 | 530/536 | 311-348 | 62.6 | Rubble | 5% | 18% |
| 7 | 4/08/14 | 15 | 531/534 | 452-592 | 62.8 | Rubble | 8-10% | 11-12% |
| 8 | 4/28/14 | 15 | 554/545 | 482-603 | 43.2 | Chunk | 9 – 12% | 13 – 16% |
| 9 | 5/7/14 | 350 | 549/423 | 389-598 | 52.5 | Chunk | 6-7% | 18 – 19% |
| 10 | 5/19/14 | 15 | 557/567 | 509-606 | 45.9 | Chunk | 10-12% | 14 - 16%* |

1 SS: steady state. "Inside" indicates temperatures measured inside the coal particles, and "all" includes temperatures measured inside the coal particles as well as temperatures measured on the surface of the particles.
2 For the later runs, we were able to estimate gas yields by two different methods (by difference between coal mass, char, and liquids, and by a dry gas meter). Consequently, we present a range of yields for these runs.

**Simulation studies**

For in-situ production, heat transfer through the coal seam is a key factor for production of products. The heat transfer dictates rate of conversion and therefore the overall mass of products. A common simulation tool for in-situ processes is a reservoir-type approach (e.g. fluid flow through porous media). While this approach has its advantages (such as computational speed and simplicity), at times it is insufficient to resolve key physics affecting production rates. This task takes a novel approach − applying CFD-based HPC computational tools to in-situ thermal treatment of coal. This approach, while computationally more expensive, is able to incorporate the fine granularity of physics required to predict heat transfer throughout the formation on the order of years and therefore provide an estimate of the production rates.

Work under this task focused on simulations of a representative section of a rubblized coal bed, which were able to capture the relevant physical processes. To perform these simulations the investigators developed a geometry creation strategy for the representative section of rubblized coal bed, appropriate boundary conditions, and a new solution algorithm to take advantage of the differing time scales. Using these strategies, a long-term thermal history of the coal seam was predicted.

The investigators selected STAR-CCM+ to perform the simulations. This commercially available software tool was developed to handle complex geometries, and it can model the convective currents through the channels of a rubblized bed of coal. STAR-CCM+ also includes Discrete Element Method (DEM) solver, which is able to simulate random coal distribution inside the test domain. Furthermore, STAR-CCM+ scales reasonably well, anywhere from 1,000 to 3,000 cores, depending on the physics included in the simulation.

The investigators studied the effects of convective channels on heat transfer inside a representative rubblized coal bed using the operator-splitting algorithm. The first step was to create a new rubblized coal geometry. The representative domain was 1 m by 1 m by 1 m cube, and the size of convective channels was around 15 mm (0.015 m). They also constructed geometries using a solid block of coal (effective aperture size of 0 m) and an empty computational domain (infinite effective aperture size). Every computational domain included three temperature probes used to monitor the temperature at that particular location. Locations of the three probes were consistent among the different geometries. The solid and empty computational volumes are shown in Figure 5, while the computational volume with an aperture size of 15 mm is shown in Figure 6. Figure 7 shows the computational mesh to resolve the individual rubblized pieces of coal, with Figure 8 showing a close up view of the mesh on one of the pieces of coal. The mesh used to resolve the convective channels is shown in Figure 9.

Figure 5. Computational geometries of solid coal and empty volumes.

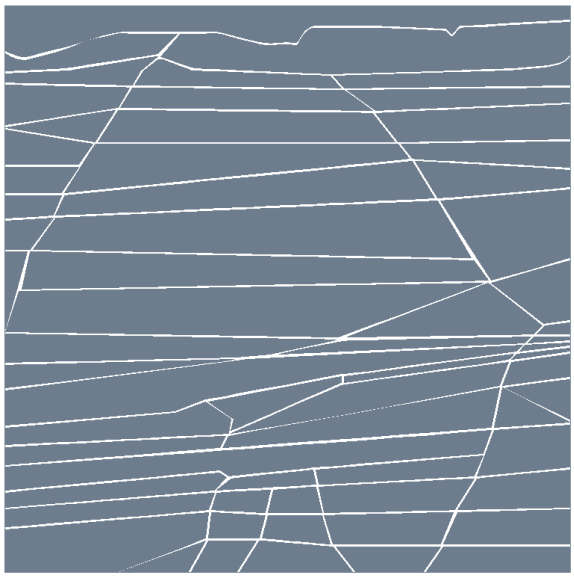

Figure 6. Representative rubblized coal geometry with aperture sizes around 15 mm.

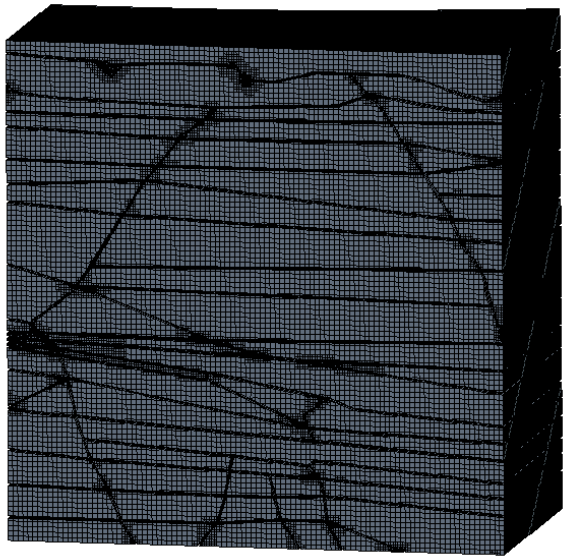

Figure 7. Mesh used to resolve individual pieces of coal.

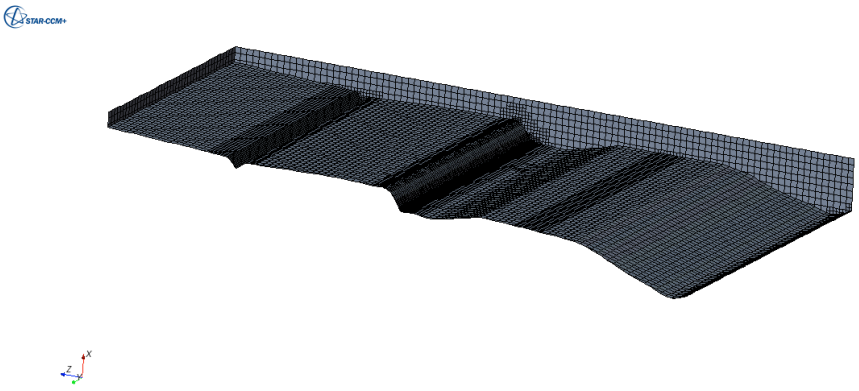

Figure 8. Close-up of the mesh for one piece of coal.

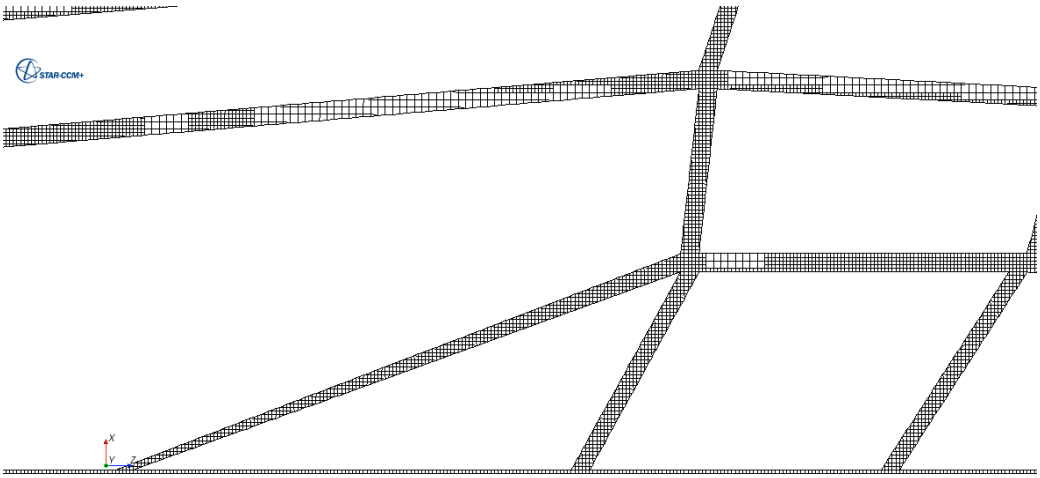

Figure 9. Close-up of the very fine mesh used to capture the fluid movement inside the convective channels, which occur between the pieces of coal (which are colored in solid white color in this figure).

For all simulations of convective channels the bottom boundary condition served as the heating source with a constant temperature of 700 K, while all other sides remained insulated. As can be seen from Figure 10 through Figure 12, the simulations are able to capture the heating inside the domain. Figure 10 shows the time temperature history of the solid coal piece, with the expected results. The lower portion of the solid domain heats up much faster than the middle or the upper portion of the coal block, as indicated by the lower probe, probe 3. After about 10-15 days of heating, the lower portion of the coal has almost reached the temperature of the heater, while the middle and upper sections are only at about 500 K. It takes about 45-50 days for the solid block of coal to reach the temperature of the heater, approximately 700 K.

In contrast, it takes less than an hour for the empty volume to reach temperature of the heater, 700 K, as shown in Figure 11. Figure 12 shows the temperature distribution inside the rubblized coal bed 15 days into heating (the temperature history data was not collected until day 15 of heating). Even at around 15-20 days into the heating, the temperatures at each of the probes show much more uniform temperature distribution than the ones seen for the solid block of coal. The results indicate the importance of convective heat transfer, which 1) greatly decreases the time required to heat the coal to the production temperature, as well as 2) heats the coal pieces more uniformly, which could have an effect on the overall quality of product.

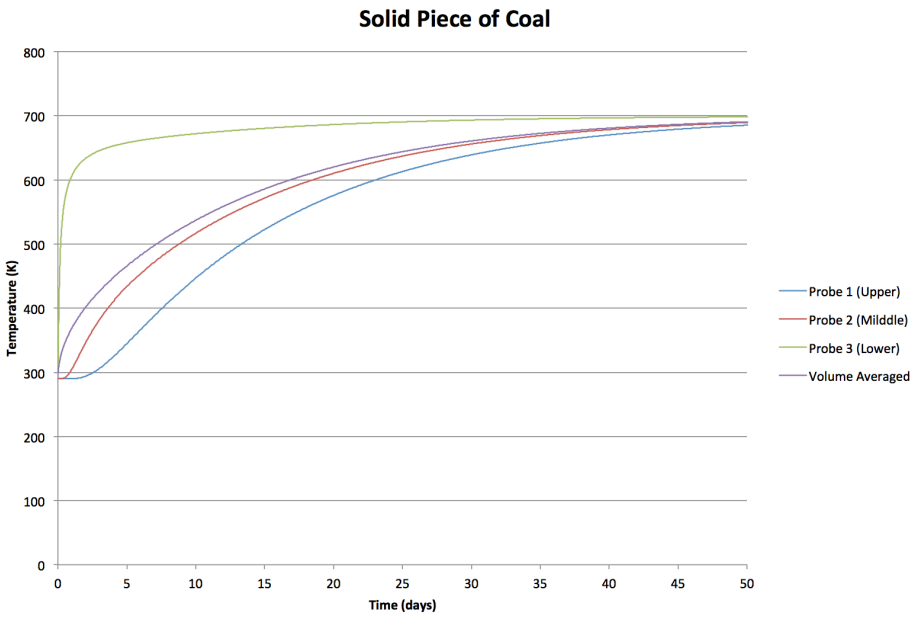


Figure 10. Thermal history plots for solid block of coal.

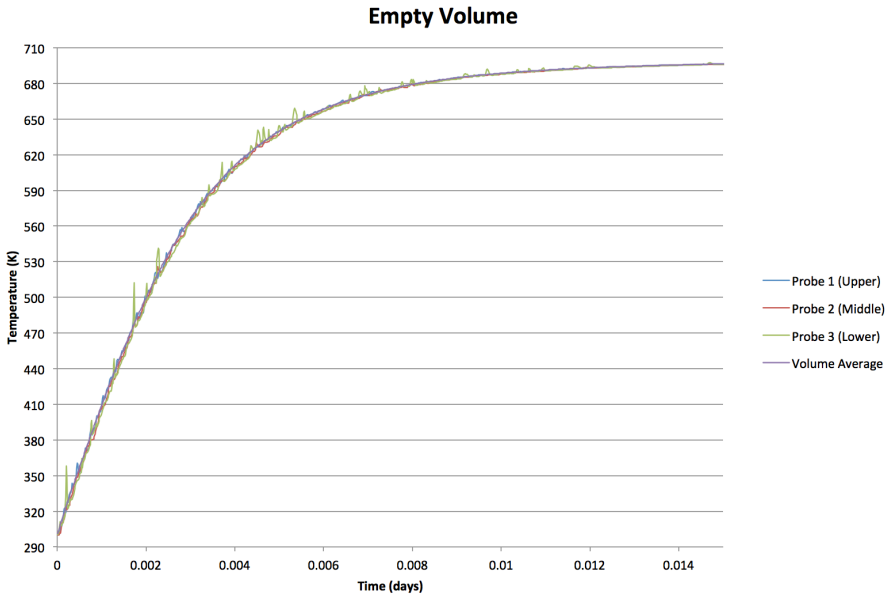


Figure 11. Thermal history plots for an empty volume geometry.

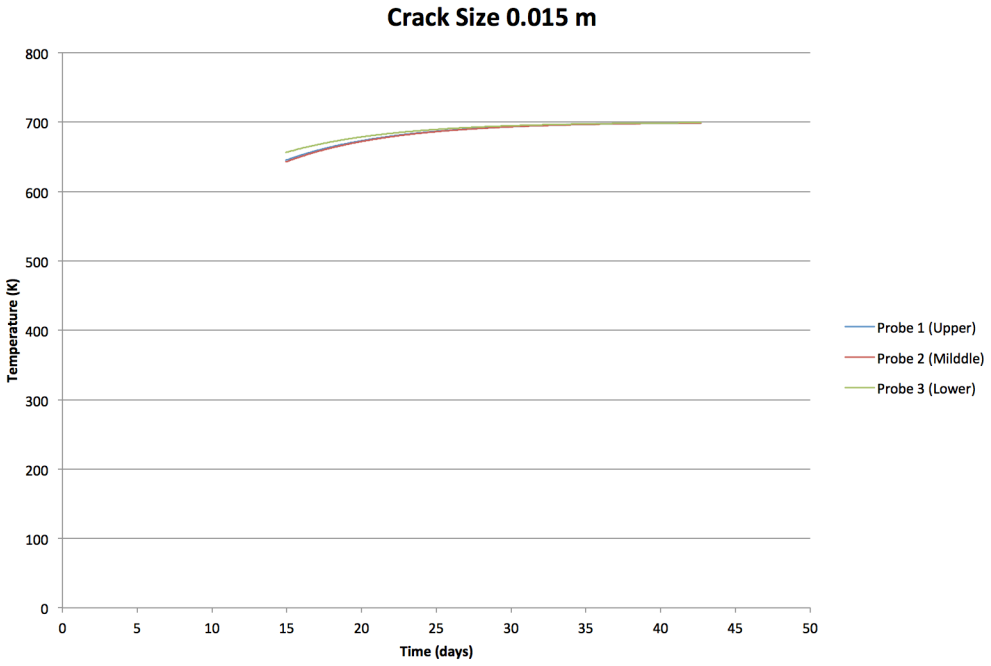


Figure 12. Thermal history plots for domain with crack sizes of 0.015 m.

**Simulations of heat transfer through coal seam**

The investigators also extended the simulations to analyze heat transfer through a seam of coal field as a representative geometry for UCTT of coal. The simulation geometry for in-situ heating was based on thickness of an actual Utah coal field, which is used as the target location for this simulation.

Upon review of available coal fields in Utah, which could serve as potential candidates for this technology, the investigators selected the Wasatch Plateau coal field as the target coal field for this simulation. The thickness of this coal field range approximately from about 6.3 ft to 14 ft, but could be as large as 30 ft. Therefore, we have picked thickness of 10 m to be represented in our simulation. To heat this coal field we use horizontal wells placed 12.5 meters apart. Different heating well orientation would not be feasible for this particular coal seam. The simulation domain shown in Figure 13 captures only a small representative section of the entire coal field, which is thousands of feet long. Therefore, the investigators use periodic boundary conditions to account for the very long coal field size. Also included in the simulation are 25 m thick zones of overburden and underburden surrounding the coal field.

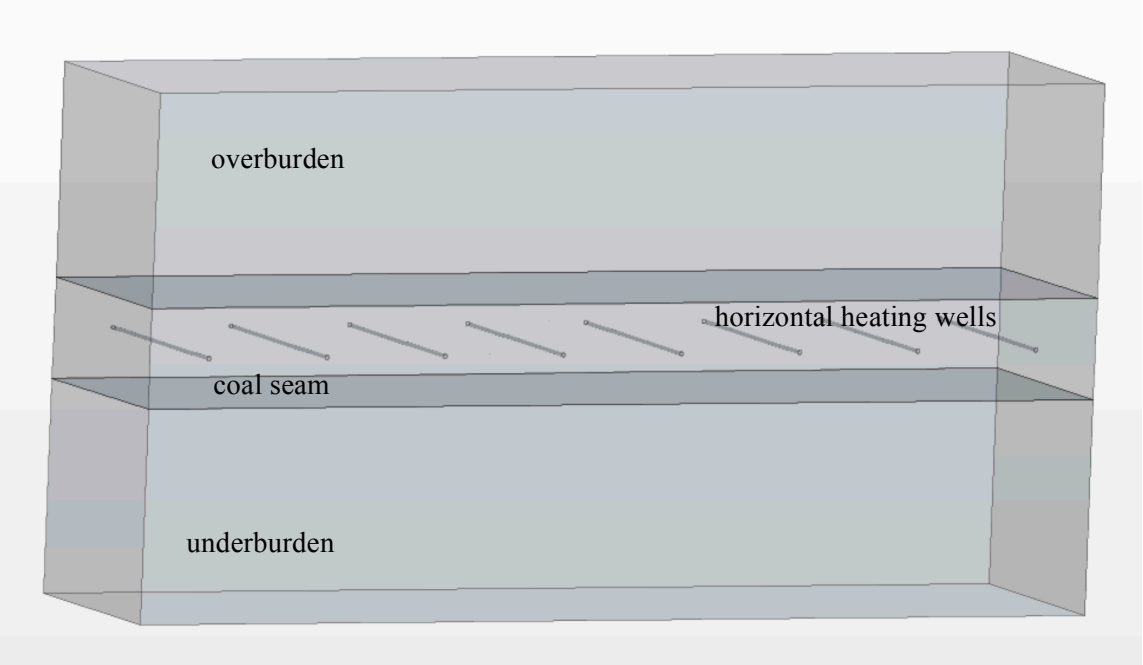


Figure 13. New simulation geometry representing Wasatch Plateau coal field with horizontal heating wells surrounded by overburden and underburden.

A very important factor for obtaining a representative temperature distribution throughout the formation is setting the appropriate physical properties for both the coal seam as well as the over/underburden. The physical properties used in this simulation were approximated from an experiments conducted under the experimental portion of this task. All physical properties are functions of temperature as well as coal conversion from raw coal to product, which is also a function of temperature. All conversions were set to change after temperature of 234 deg. C, which is the evaporating temperature of water at about 1,000 ft below surface and at pressure of about 30 bar. Utah Sufco coal has a moisture content of 3.2 %, which was used in the simulation as well.

As coal is heated it is converted to char, tars and light gases. For Utah Sufco coal, at full conversion, products and char account for 45% and 55% on mass basis, respectively. The products are assumed to be 50% liquid and 50% gas. Based on the experiments the investigators assumed the gas product is a mixture of 30% methane, 30% carbon dioxide, 30% ethane, and 10% water. The liquid properties were based on the single-carbon number analysis of the liquid product (Figure 26). Based on these compositions, ProMax™ process simulation software provided the aggregate properties of the products as a function of temperature. The aggregate physical properties used in the simulations are as follows:

Density, $r$:

$$r = 0.00281\ T^2 - 4.54\ T + 2345 \quad (kg/m^3)$$

where: $T$ is temperature in degrees C.

Thermal conductivity, $k$:

$$k = -6.13e\text{-}7\ T^2 + 4.67e\text{-}4\ T + 0.281 \quad (W/m\text{-}K)$$

where: $T$ is temperature in degrees K.

Specific heat, $c$:

$$c = 2.61e\text{-}6\ T^2 - 1.03e\text{-}4\ T + 1.23 \quad (J/g\text{-}°C)$$

where: $T$ is temperature in degrees °C.

While physical properties account for the heat transfer throughout the formation, a yield function determines the amount of product produced, and ultimately, the Net Energy Return (NER). Therefore, the yield function plays a crucial role in determining the process viability. To obtain the yield function, a sigmoidal function was used to fit the experimental yields. The resulting sigmoidal fit is given by:

$$Yield = Yield_{max} / (1 + exp\ (0.02096\ (T_{fit} - T)))$$

where: $T$ is temperature in degrees K, $Yield_{max}$ is the maximum yield, and $T_{fit}$ is the temperature constant determined from the experimental runs.

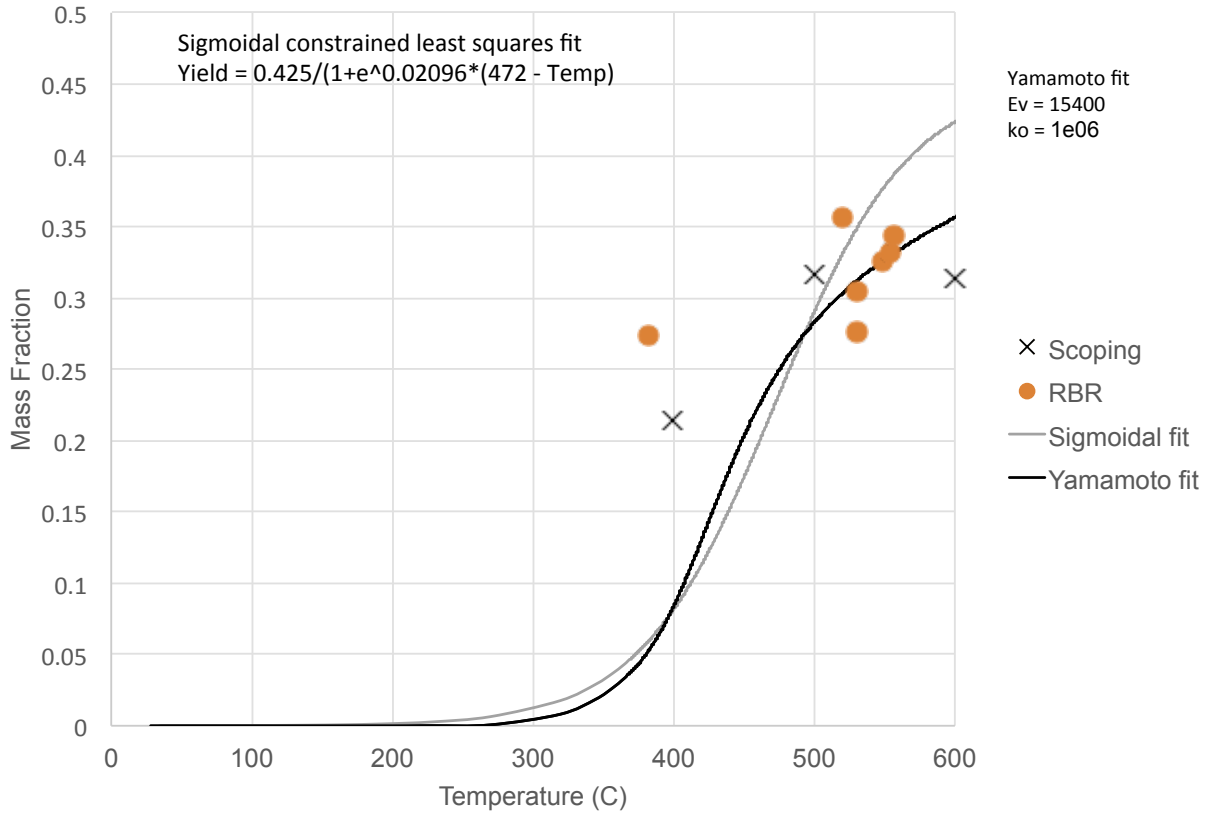


Figure 14. Fit of a sigmoidal yield function to the scoping data. The RBR results and the Yamamoto yield model fit for Sufco coal are shown for comparison.

Based on the spread of experimental yields as a function of temperature, three yield functions were considered for this study:

Yield 1: $Yield_{max} = 0.42,\ T_{fit} = 850\ K$

Yield 2: $Yield_{max} = 0.54,\ T_{fit} = 620\ K$

Yield 3: $Yield_{max} = 0.4525,\ T_{fit} = 745\ K$

The Yield 1 function represents the lower, more conservative yield relationship; Yield 2 represents the upper, more optimistic yield relationship. Yield 3 represents the base fit, which is in between the more optimistic and more conservative scenarios. Each yield function was used in a separate simulation to determine the appropriate mass of product and therefore NER for that particular scenario. Also considered were two other cases, both with the Yield 3 model. One of these additional cases assumed that the coal seam is about 60 m thick, and the last case used a lower heater temperature of 675 K. All of the previous cases (heat transfer in a coal seam) use heater temperature of 1073 K, which is relatively optimistic for underground thermal heating. The initial formation temperature for all simulations was set to 310 K.

Before running these simulations in STAR-CCM+, the investigators performed a verification study on a simplified geometry inside STAR-CCM+ for which there is both an analytical solution as well as an easy numerical implementation in a programming language such as Fortran. For the verification study the investigators have chosen to use an unsteady heat transfer in an infinite annulus with specified temperatures at both the inner and outer boundaries. The inner radius of the annulus was set to 0.25 m and the outer radius to 35 m. The inner temperature boundary was held at 1073 K, same as the temperature of the heaters for the UCTT study, while the outer temperature was held at 310 K. The unsteady heat equation in Cartesian coordinates is of the form:

$$\frac{1}{\alpha}\frac{\partial T}{\partial t} = \frac{\partial^2 T}{\partial x^2} + \frac{\partial^2 T}{\partial y^2}$$

Comparing the numerical implementation in Fortran with the results with STAR-CCM+ revealed that the temperature profiles are identical (Figure 15). This exercise was helpful in verifying STAR-CCM+ algorithms and their suitability for use in approximating thermal profiles inside a more complicated geometry containing various heaters, for which there is no analytical solution or easy numerical implementation in an external program.

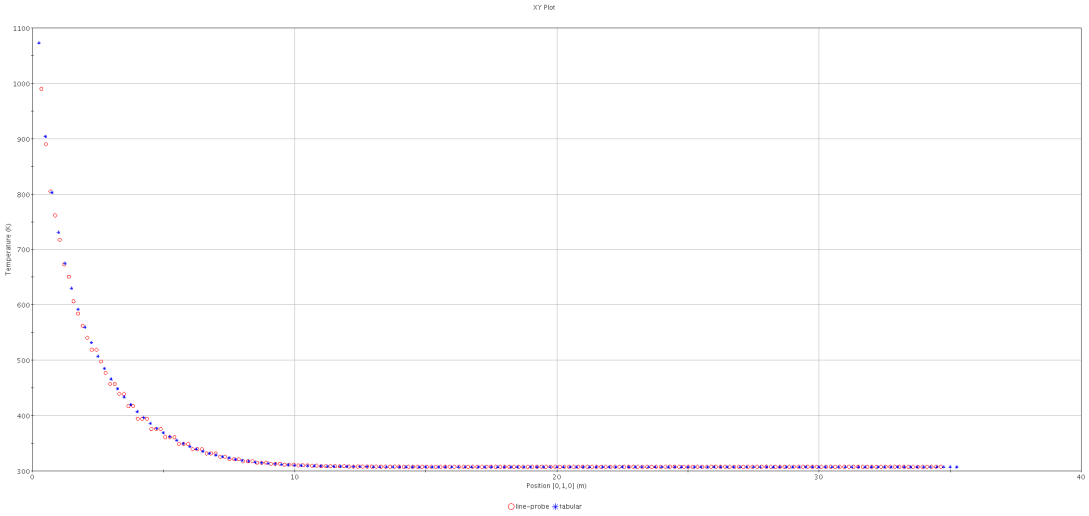


Figure 15. Temperature profile comparison for a verification study. The red circular symbols represent results from STAR-CCM+, whereas the blue star symbols are temperature results obtained from an external numerical implementation of the unsteady heat equation.

Also, the investigators performed a scaling study to determine the optimal number of processors for the UCTT simulations. Results of the scaling study are shown in Figure 16. The speed up was determined by taking the performance on 360 cores as the basis. As can be seen, STAR-CCM+ shows nearly a linear speed-up up to 3,000 cores for a representative UCTT simulation, which includes conductive heat transfer

physics with variable properties. Therefore, doubling the number of cores results in decreasing the computational time by a factor of two.

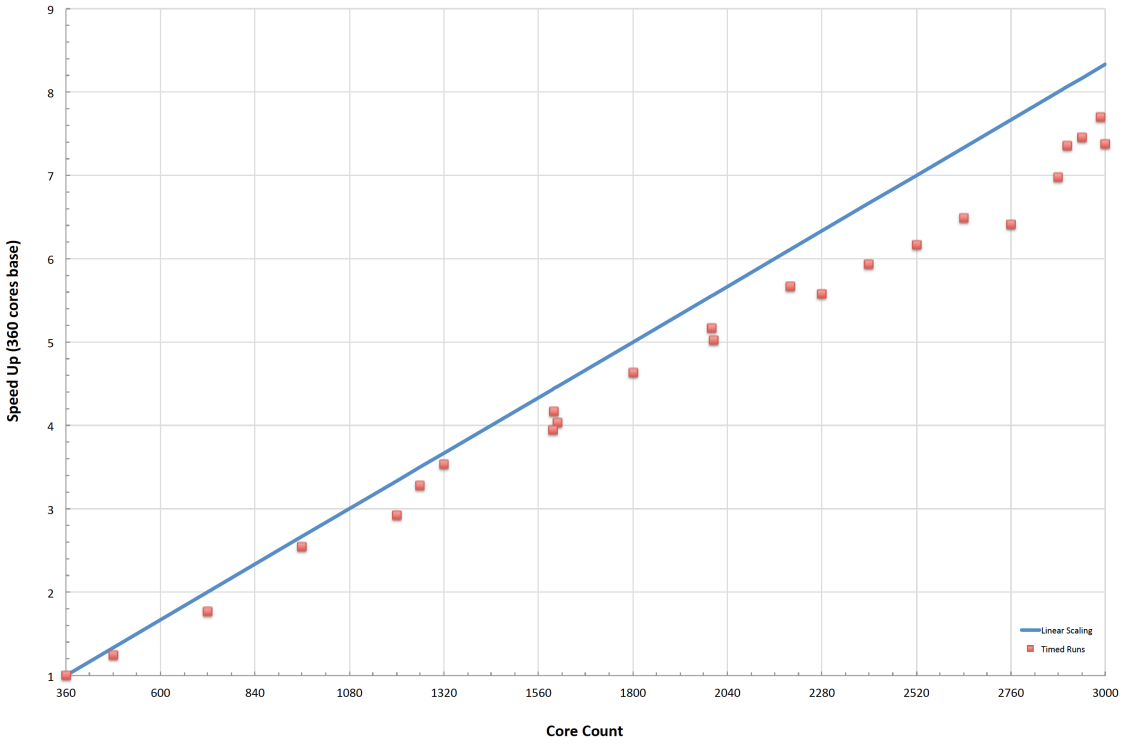


Figure 16. Scaling results for STAR-CCM+ and a representative simulation domain for UCTT.

## $CO_2$ storage studies

The intent of this subtask is to describe the adsorption of methane and carbon dioxide on a coal that has undergone pyrolysis with slow heating rates. Underground coal pyrolysis is a process similar to *in situ* oil shale production wherein heat is applied to deep coal formations to produce light hydrocarbons. Like enhanced coal bed methane, the injection of $CO_2$ post thermal treatment can improve hydrocarbon recovery and serves as a means of carbon storage. Little information exists pertaining to coals pyrolized to temperatures expected with this process. This subtask specifically examines the development of meso- and micropores and their influence on methane and carbon dioxide adsorption on thermally treated coals. It also examines where some of the meso- and micropores reside and the means of their development. Finally, it attempts to show a relationship between small pores and adsorption.

Carbon dioxide storage plays a crucial role to the UCTT process. If carbon emission regulations become reality in the United States, it may be advantageous to offset some of the carbon that is emitted while heating up the coal formation by permanently sequestering it. This study helps prove the concept that $CO_2$ could be stored in the pyrolized coal. The pyrolysis of coal results in several changes to the coal including the potential increase in meso- and micropores as well as an increase in adsorptive capacity (Maroto-Valer et al. 2005). The purpose of this study is to quantify some of changes in meso- and

micropores and determine how the changes in these pores affect the overall adsorption of methane and $CO_2$. The main goal of this subtask is to provide high-pressure adsorption isotherms under reservoir temperatures.

Three different coals were examined in this study: a Utah bituminous coal from the Sufco/Skyline mine in Utah, an Illinois bituminous coal from the Carlinville mine, and a Powder River Basin (sub-bituminous) coal from the North Antelope mine near Gillette Wyoming. In the following text, the individual coals will be referred to by the mine from which they were sourced. These coals were chosen for several reasons. The Sufco coal was chosen primarily for its high levels of volatile matter and relatively low sulfur. It was also chosen to retain consistency with the other subtasks. Sufco coal is representative of much of the bituminous coals in Utah. The Carlinville coal was chosen to represent some of the high-sulfur bituminous coals near the northern Appalachians. The North Antelope coal was chosen to further diversify the scope of this study; Powder River Basin coals have some interesting properties such as very low sulfur and very high moisture contents. All three coals can be found in either shallow mineable formations or in deep unmineable seams that would be target candidate for UCTT.

All of the coals used for this study were already crushed to approximately 20 mm chunks. The coals were sampled before being stored in opaque airtight containers in a climate-controlled room. Approximately 5kg of each coal was procured for experimentation. Elemental, heating value, moisture, ash content, and volatile analysis can be found in Table 4.

Table 4. Coal properties. All values are reported on a percentage by weight basis except for the Higher Heating Value (HHV).

| | Sufco | Carlinville | North Antelope |
|---|---|---|---|
| Loss on drying (105°C) | 3.18 | 9.65 | 23.69 |
| Ash (750°C) | 8.83 | 7.99 | 4.94 |
| C | 70.6 | 64.67 | 53.72 |
| H | 5.41 | 5.59 | 6.22 |
| N | 1.42 | 1.12 | 0.78 |
| S | 0.53 | 3.98 | 0.23 |
| O (by diff.) | 13.21 | 16.65 | 34.11 |
| Volatile matter | 38.6 | 36.78 | 33.36 |
| Fixed carbon | 49.39 | 45.58 | 38.01 |
| HHV (btu/lb) | 12606 | 11598 | 9078 |

Pyrolysis of the coal samples was performed in a 64mm clamshell-style tube furnace 24 inches (61 cm) in length. The tube furnace used was a Thermo Scientific Lindberg Blue controlled using an Omega CN1504 programmable process controller. Power was supplied to the heaters by a 240V three-phase wall outlet passing through a 30 ampere solid-state relay.

A long protrusion was cooled with a fan and served to condense out some of the oils produced during heating. Plumbers unions were attached to both ends of the reactor to facilitate loading and unloading the tube furnace. With the use of sequentially reducing fittings, the ultimate diameter on the inlet was 0.25 inches (6 mm). A quarter inch Swagelok tee facilitated the injection point for gas and mounting point for a k-type thermocouple that ran longitudinally through the reactor to the center of the heated zone. Gas

was supplied from a k-type cylinder through the appropriate regulator and controlled with a calibrated rotometer. Figure 17 is a process flow diagram for the pyrolysis apparatus.

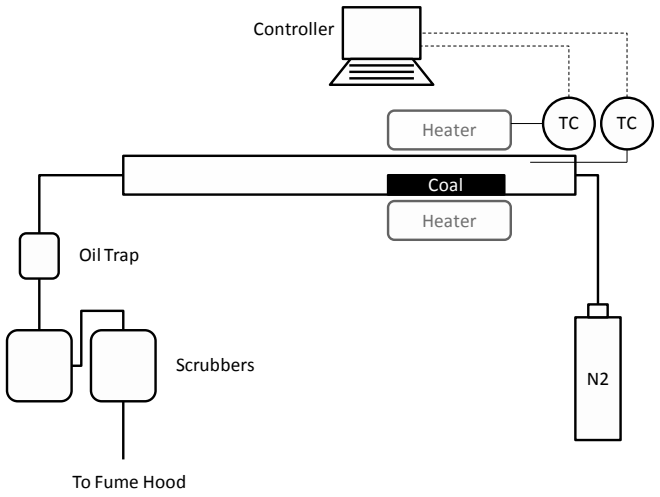


Figure 17. Schematic of the tube furnace used for producing the coal samples. The furnace has an internal diameter of 2.5 inches and a heated length of 2 feet. There is a four foot unheated section to facilitate cooling of the oils and gases.

Ultimate pyrolysis temperatures of 325, 450, and 600°C were chosen as likely temperatures encountered with UCTT. Multiplying the different treatment temperatures with the different heating rates for three different coals plus three unreacted coal samples resulted in 21 samples overall (Table 5).

Table 5. Summary of all of the coal samples prepared for analysis.

| **Skyline** | | **Carlinville** | | **North Antelope** | |
|---|---|---|---|---|---|
| Unreacted, Dry | | Unreacted, Dry | | Unreacted, Dry | |
| 325°C @ 10°/min. | 325°C @ 0.1°/min. | 325°C @ 10°/min. | 325°C @ 0.1°/min. | 325°C @ 10°/min. | 325°C @ 0.1°/min. |
| 450°C @ 10°/min. | 450°C @ 0.1°/min. | 450°C @ 10°/min. | 450°C @ 0.1°/min. | 450°C @ 10°/min. | 450°C @ 0.1°/min. |
| 600°C @ 10°/min. | 600°C @ 0.1°/min. | 600°C @ 10°/min. | 600°C @ 0.1°/min. | 600°C @ 10°/min. | 600°C @ 0.1°/min. |

The isotherm measurement apparatus is identical in design to that used by Mavor et al. (1990), which was a volumetric/manometric type. The advantages of a volumetric/manometric apparatus include (Keller and Staudt 2005): 1) Simplicity, volumetric measurements do not require complicated or expensive equipment. 2) Data reduces well if the mass of the sorbent is known and the calibration is maintained. Disadvantages of volumetric/manometric measurements are: 1) Volumetric measurements require more material than other measurement techniques. 2) A long time may be required for the adsorption system to come to equilibrium. 3) Volumetric measurements give little insight into the kinetics of adsorption.

The isotherm apparatus used custom machined reference and sample cells rated to 690 bar at 100°C made out of polished stainless steel. Using polished material reduces the amount of adsorption on the walls of the apparatus thereby reducing experimental error (Keller and Staudt 2005). All fittings and connections in the apparatus are from Autoclave Engineers and are 0.25 inch (approx 6mm). Fittings and tubing used for the apparatus are rated to over 690 bar. High pressure needle valves were used to contain pressure. Pressure was monitored using Honeywell TJE pressure transducers with an effective range from 0 to 690 bar. The voltage outputs from the pressure transducers were transmitted to a custom TerraTek signal conditioner and from there to a Dell Optiplex 755 personal computer via serial cable and data acquisition card. Pressure readouts were recorded using TerraTek software, Isotherm Legacy built using LabView software.

Three identical reference cell and sample cell isotherm systems were used in parallel. Due to the long time necessary for the isotherm system to come to equilibrium (hours to days per data point), running three isotherm measurements simultaneously was more efficient. A schematic of a single reference cell and sample cell system can be found in Figure 18.

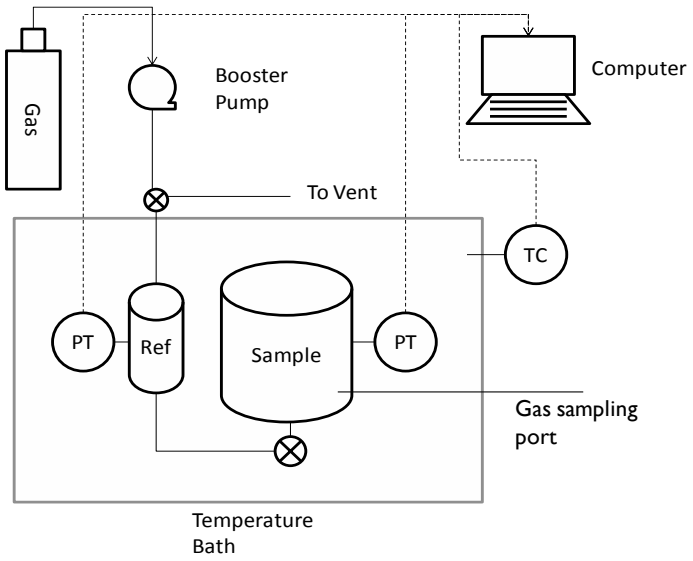


Figure 18. Schematic of a single sample cell and reference cell used to measuring isotherms. The isotherm apparatus at TerraTek has three identical sample cell and reference cell systems.

All of the isotherm measurement units were placed in a custom-made stainless steel bath filled with Xiameter, a Dow-Corning silicone-based fluid selected for its low vapor pressure and high temperature stability. The temperature of the bath was controlled using a VWR 1122s immersion heater/circulator.

Measurement on each coal sample involved two different gases ($CO_2$ and $CH_4$) at two different measurement temperatures (50°C and 70°C) resulting in four isotherm measurements for each sample (Table 6). Measurement temperatures were chosen as reasonable approximates of an unmineable coals *in situ* temperature.

Table 6. Experimental matrix for isotherm measurements on each sample.

| | Adsorptive | |
|---|---|---|
| Temperature | $CO_2$ | $CH_4$ |
| 50°C | 1 | 3 |
| 70°C | 2 | 4 |

## RESULTS AND DISCUSSION

### Experimental studies

#### Scoping studies

Figure 19 shows the gas, liquid and solid product yields for scoping studies. As shown in the figure, higher final temperatures result in more gas and water, and less solid product. These higher temperatures cause more conversion of coal to liquid and gas products. However, there is no clear difference between 500°C and 600°C, which can give an indication of the best conditions for return on investment. For the effect of pressure and heating rate, no clear conclusions can be derived based on the conditions studied and data obtained.

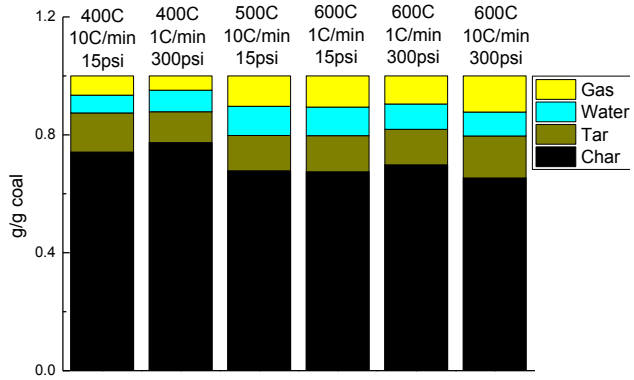


Figure 19. Gas liquid and solid product yield for scoping studies. Yield is on a dry basis (not ash free, since the ash content of our samples varied dramatically).

Figure 20 shows the gas-phase product yields at various conditions. These data illustrate that increasing the final temperature from 400-500°C increases the yield of $CH_4$, CO, $H_2$ and $CO_2$. Only the $H_2$ yield significantly increases from 500-600°C. Pressure appears to inhibit yield of all gas-phase species except $CH_4$ and $CO_2$, but this factor does not appear to be as important as the final temperature.

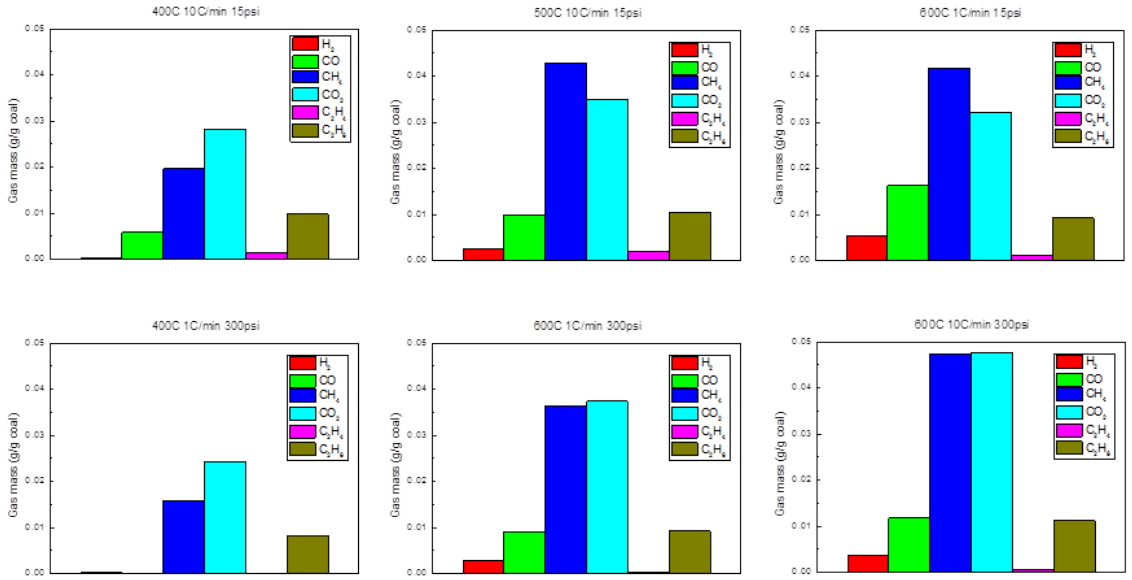


Figure 20. Gas-phase product yields at various conditions.

Figure 21 shows the composition of liquid products for selected experiments based on a normalization method, which assumes that all compounds are identified and the area of all peaks sums to 100%. As shown from the figure, more than 50% of the tar products are paraffins. Increasing the final temperature increases the percentage of aromatics, but the aliphatic content remains high. Increasing the pressure appears to increase the generation of lower molecular weight products, which is not unexpected.

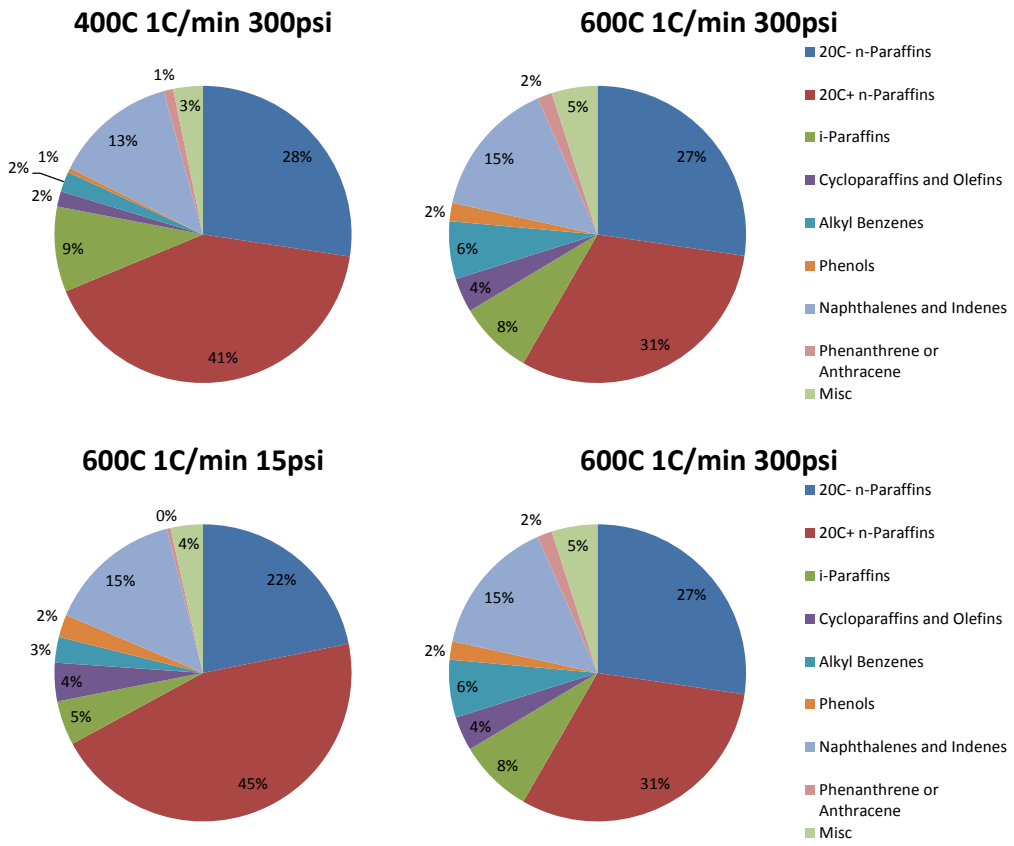


Figure 21. Composition of liquid products for selected experiments.

**RBR studies**

*Yield and products*

Figure 22 shows typical gas-phase concentrations and the coal internal temperature profile. Note that the coal internal temperature used is the top center thermocouple located in the middle coal chunk. The most abundant gas-phase products are methane and $CO_2$, followed by CO, ethane, ethylene, and hydrogen. Measured gas products include $H_2$, CO, $CH_4$, $C_2H_4$, $C_2H_6$, and $CO_2$. The results in Figure 22 are typical of the runs at ambient pressure and at temperatures above 500°C.

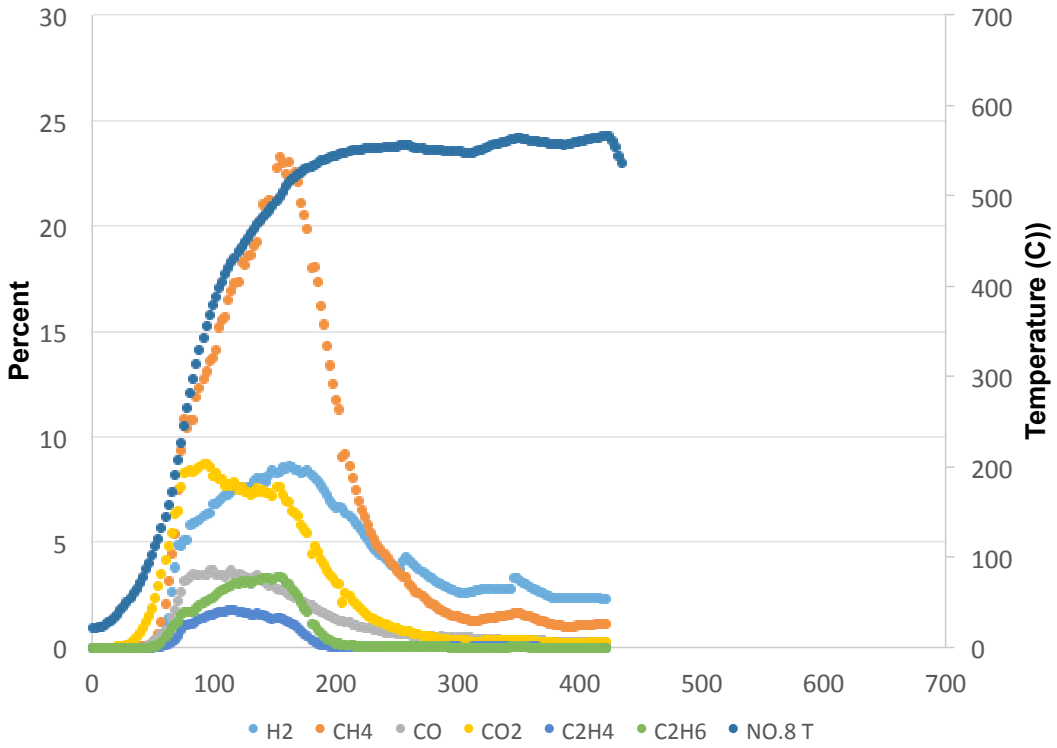


Figure 22. Temperature and gas-phase concentrations for run #8, heater set point at 800°C, ambient pressure, and a coal internal steady-state temperature of approximately 550°C (run #8). The percent on the y axis is volume percent.

Figure 23 summarizes the yields for the scoping and RBR studies. It shows that yield increases with temperature, as expected, and that the yields for the scoping and the RBR studies agree reasonably well. The effect of pressure on yield is less clear from the results. At temperatures of at or greater than 500°C, yields ranged from 20 – 28% (excluding water) on a dry basis.

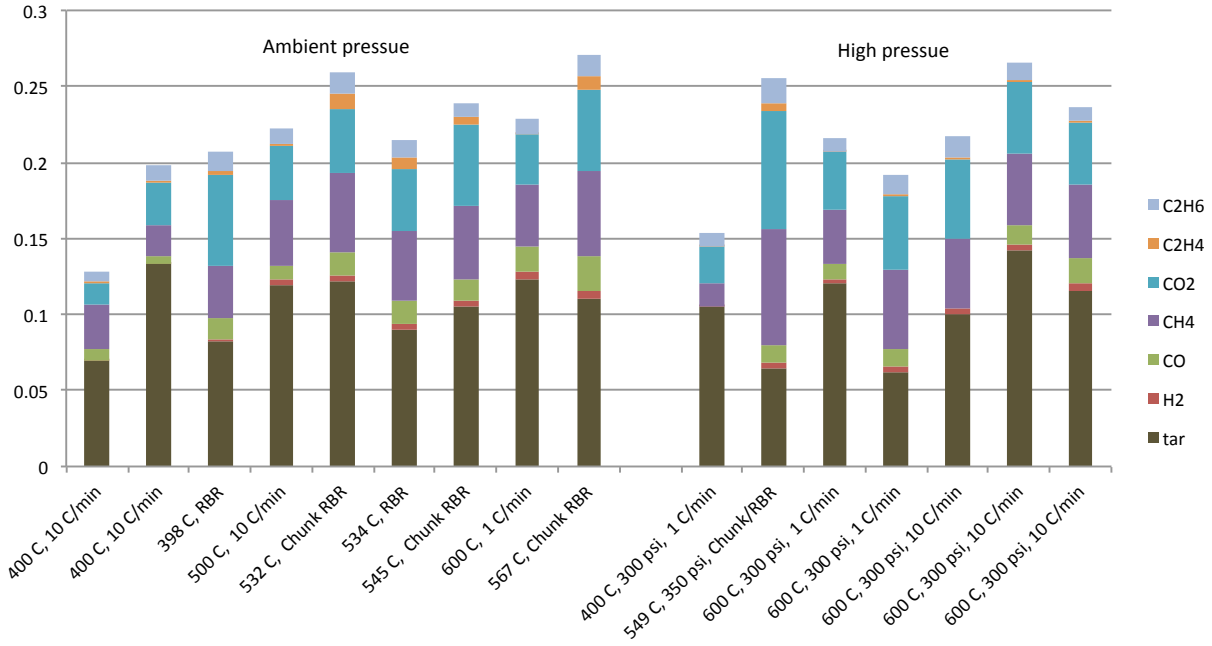


Figure 23. Summary of yield results for the scoping and RBR studies. The left side indicates ambient pressure runs, and the right side indicates high-pressure runs.

The liquid products included C7 and heavier compounds. Figure 24 shows the simulated distillation results from the liquid product sample for run #3 (heater at 800°C), and Figure 25 shows results for a crude oil reference simulated distillation obtained by the same method. The two figures illustrate that the UCTT product is light-crude like, but it contains doublets, which means that many of the carbon peaks show both a single and double-bonded species, i.e., decane and decene, whereas the crude reference sample does not tend to show doublets, i.e. only decane. Consequently, the UCTT product is less saturated and more reactive than conventional crude, which is not unexpected from a thermally derived product. Figure 26 shows that the most common species in the product mix range from C8 – C15. Although the single-carbon number results indicated assume 100% detection, and the sample likely contains 20% residual materials, it still provides a good indication of the product composition.

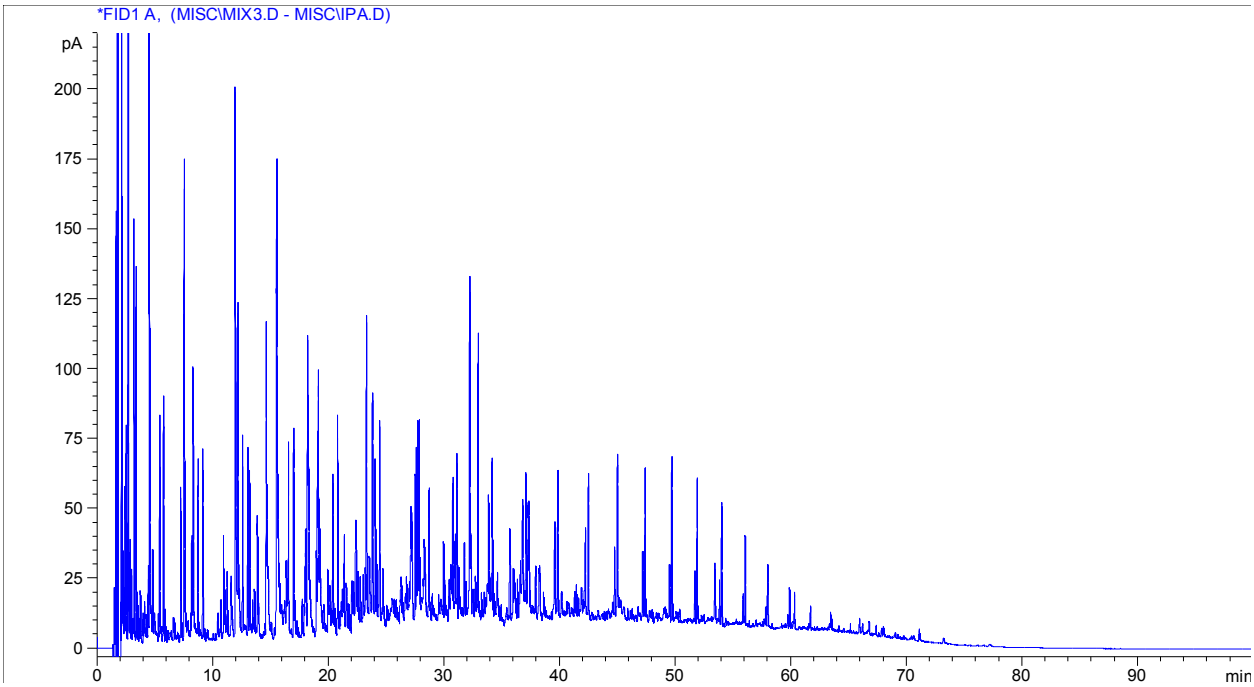

Figure 24. GC-FID analysis of RBR liquid product from run #3.

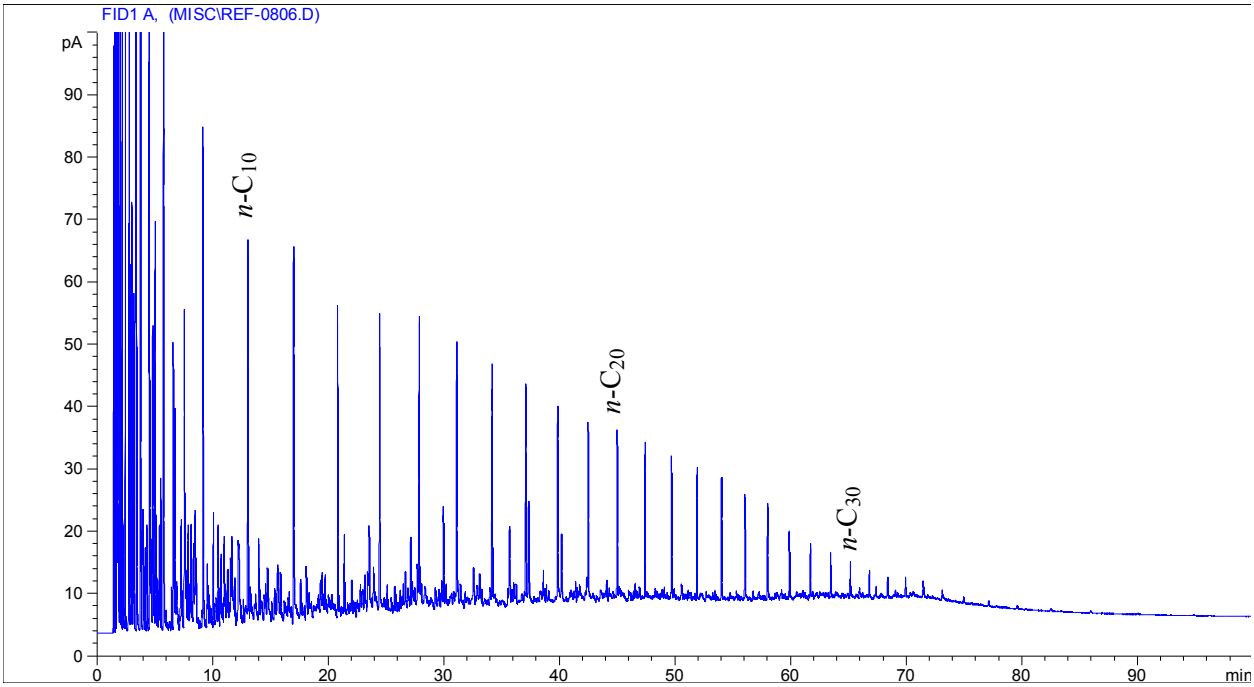

Figure 25. GC-FID analysis of crude oil reference.

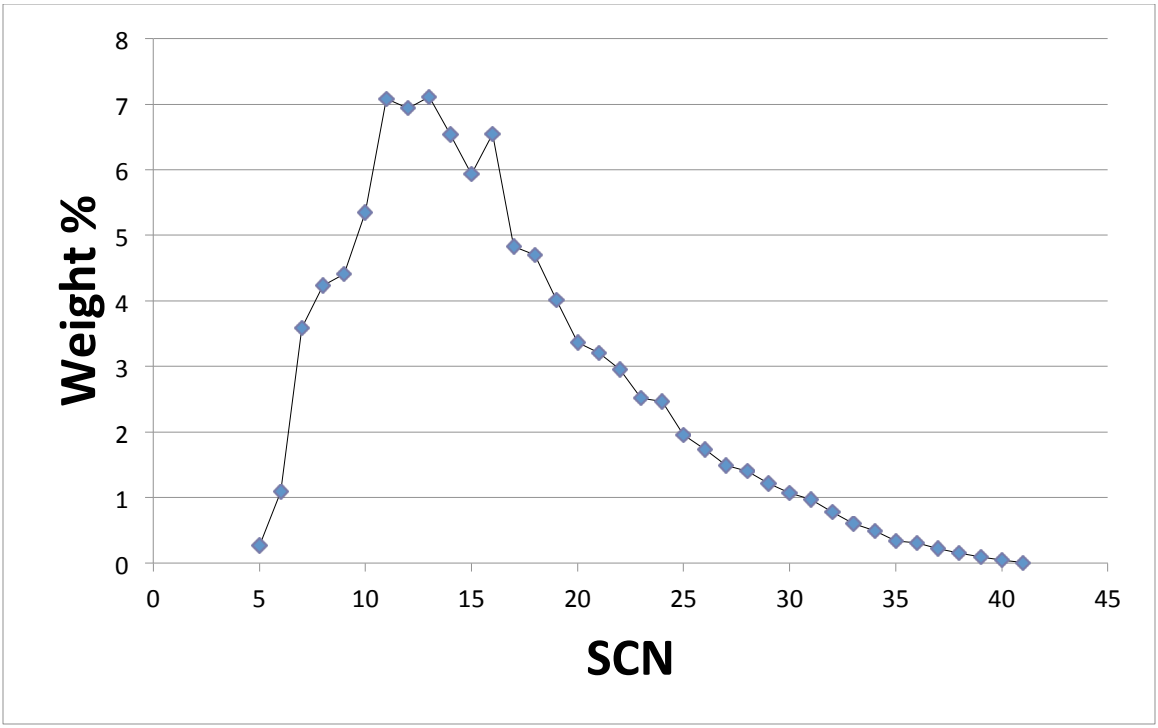

Figure 26. Single carbon number (SCN) weight distribution.

There are some products between C3 and C7, which are not captured by this system, but a brief study found these to be insignificant.

*Material balance*

Figure 27 and Figure 28 show the mass balance for Run #3 and how the species partition between char, tar, gas-phase products, and water. Note that this balance uses the average coal composition (Table 1), elemental analysis of the liquid and gas-phase samples from Run #3, and the char composition for all similar RBR runs. Approximately six percent of the hydrogen and twenty percent of the oxygen are from the original moisture in the coal (mole %). Approximately 3% of the carbon and 6% of the hydrogen are not accounted for in the balance. Because nitrogen was not measured in the liquid product, the investigators assumed that any remaining nitrogen partitions to the tar. Both the oxygen and the sulfur balances slightly over-account for these species. This result is likely due to the inhomogeneity of the coal.

Both of these figures show that carbon tends to partition to the char, while hydrogen tends to partition to the gas and tar products. Oxygen tends to be found in the water and gas products, while sulfur tends to partition to the char and tar products.

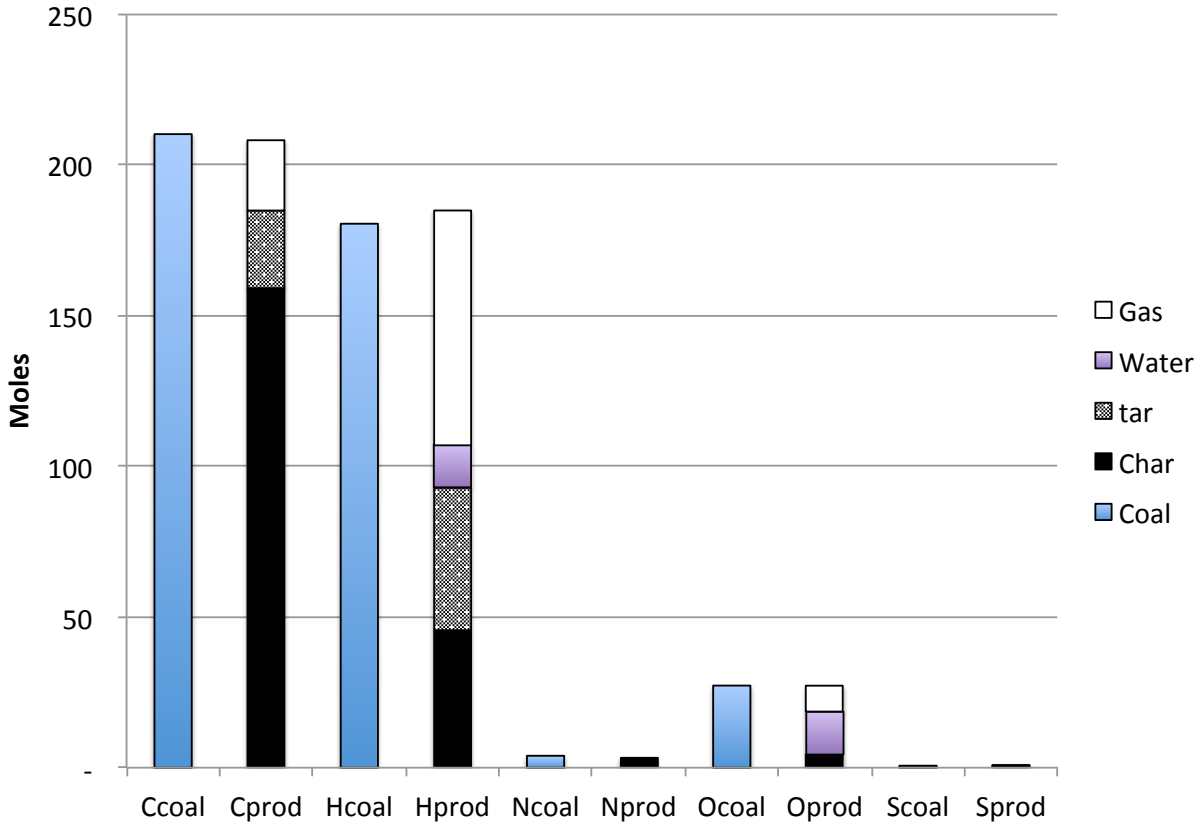


Figure 27. Moles of carbon (C), hydrogen (H), nitrogen (N), oxygen (O), and sulfur (S) in the original coal (as received) and in the char, tar, and gas.

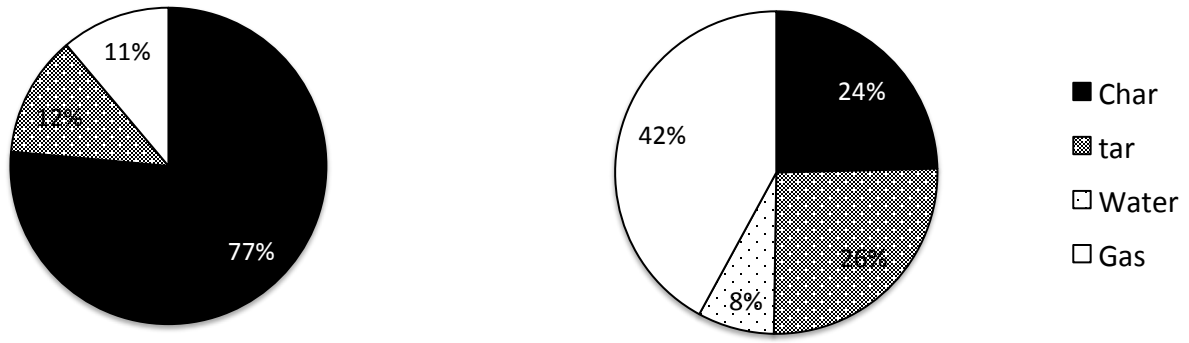


(a) (b)

Figure 28. Distribution of carbon (a) and hydrogen (b) among the char, tar, water and gas phases (mole %).

Because the coal chunks are large and only heated on one side, the coal closest to the heater tends to be more thoroughly pyrolized than the coal further from the heater. Figure 29 illustrates how the fixed carbon content increases and the volatile content decreases for char samples that are closer to the heater (bottom). This trend is apparent for both the ambient pressure and elevated pressure runs.

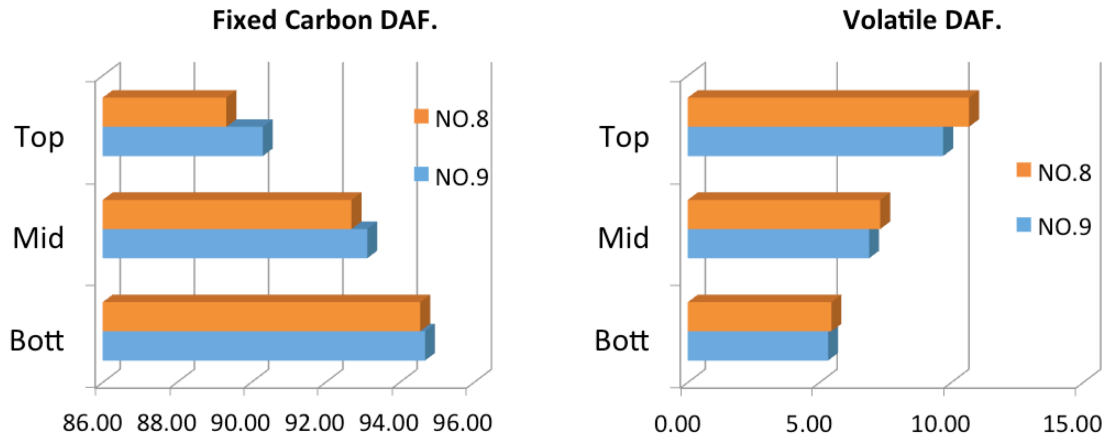


Figure 29. Comparison of fixed carbon and volatile matter content for run number 8 (ambient pressure).

**Simulation studies**

After completing our verification and scaling studies, the investigators ran five simulations comparing the various yield models as well as seam thicknesses and heater temperatures. An example temperature distribution as well as production rate for Yield 2 model after 1,800 days of heating are shown in Figure 30 and Figure 31, respectively. Similar temperature and yield profiles are obtained for the other four simulations. Perhaps the largest difference in temperature and yield profiles is seen for the Yield 3 model coupled with the lower heater temperature of 675 K. The temperature and yield profiles are shown in Figure 32 and Figure 33. As can be seen, the temperatures throughout the formation for Yield 3 model with lower heater temperatures are much lower than temperatures for the remaining four simulations with heater temperatures of 1073 K. Because of the lower temperatures, there is also less product produced over the considered time period of 1,800 days, or about 5 years of heating. These differences have significant impact on the overall NER of the process.

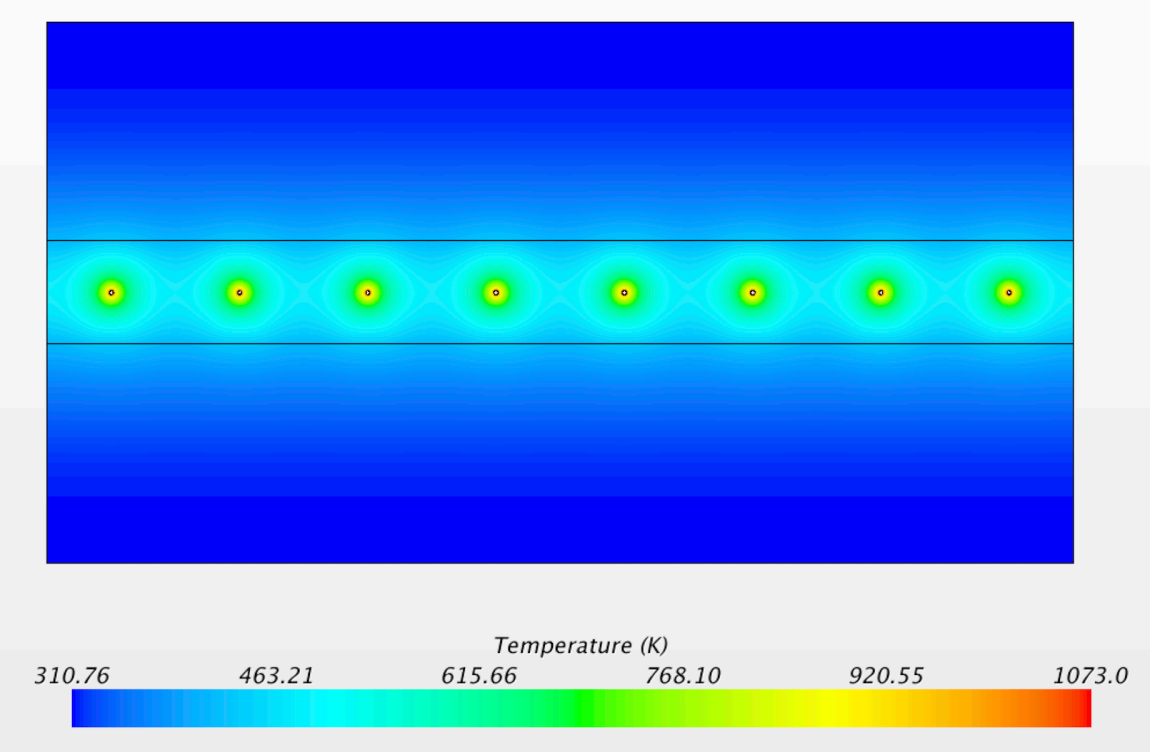


Figure 30. Front view of a temperature distribution inside the coal seam surrounded by overburden and underburden for Yield 2 model after 1,800 days of heating.

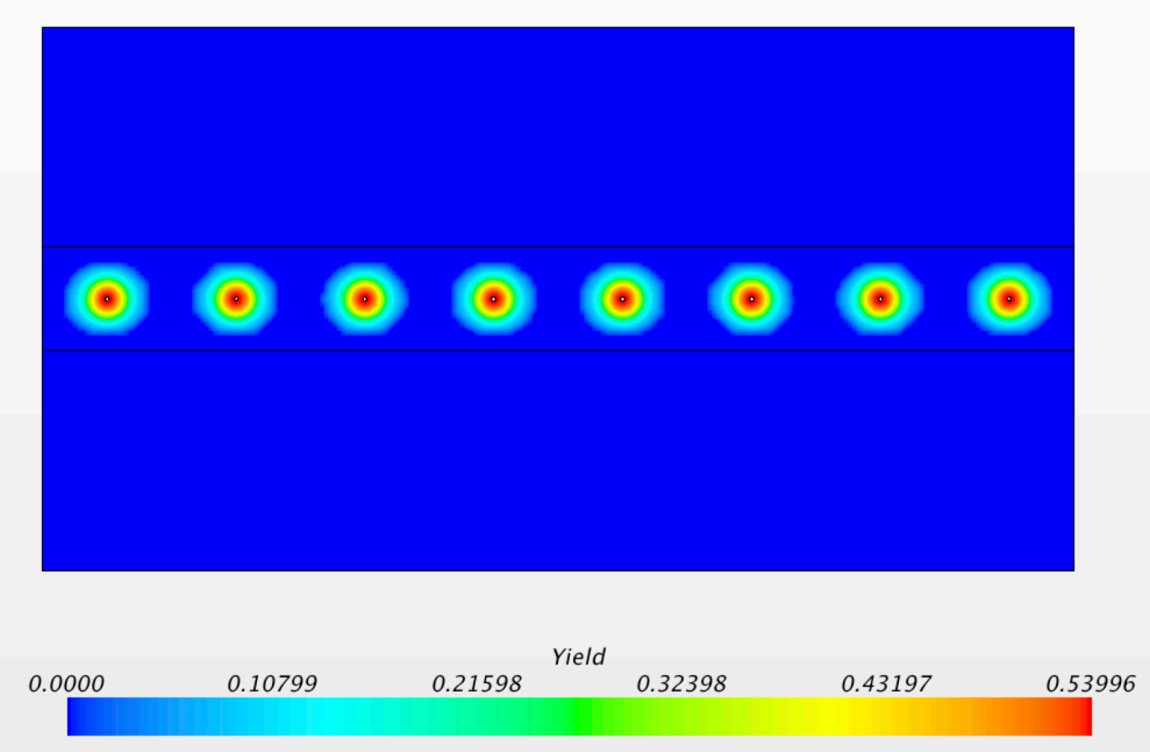


Figure 31. Front view of a yield distribution inside the coal seam for Yield 2 model after 1,800 days of heating.

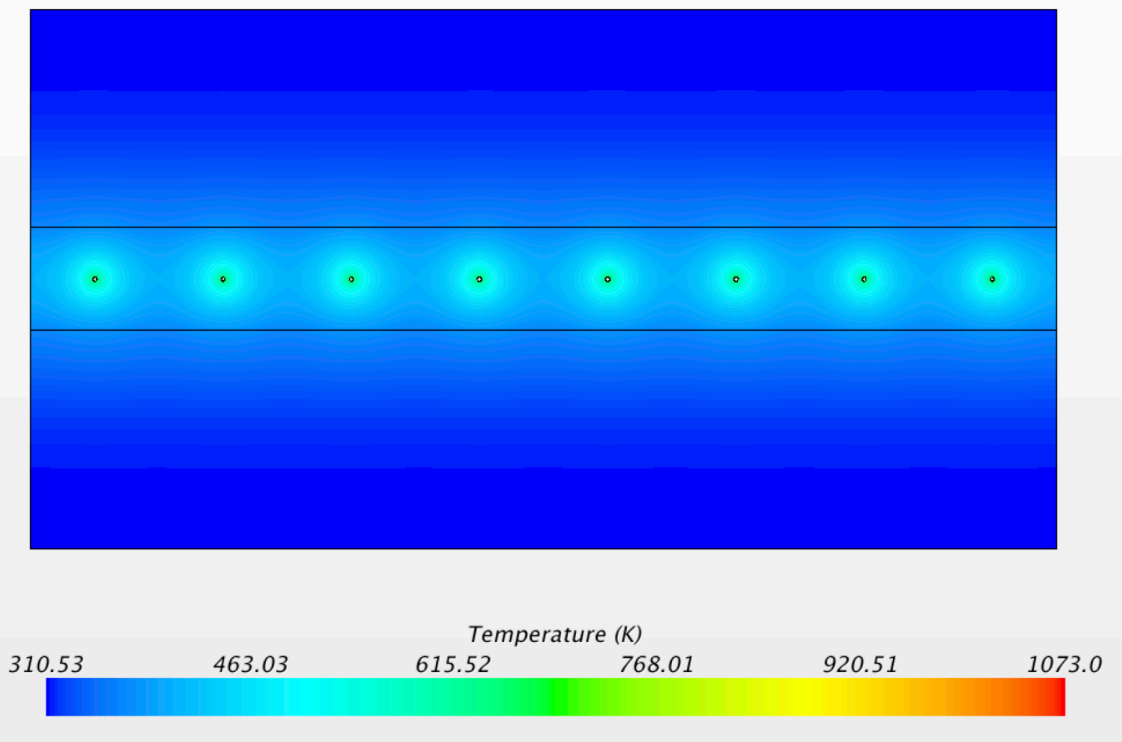


Figure 32. Front view of temperature distribution for Yield 3 model with lower heater temperature of 675 K after 1,800 days of heating.

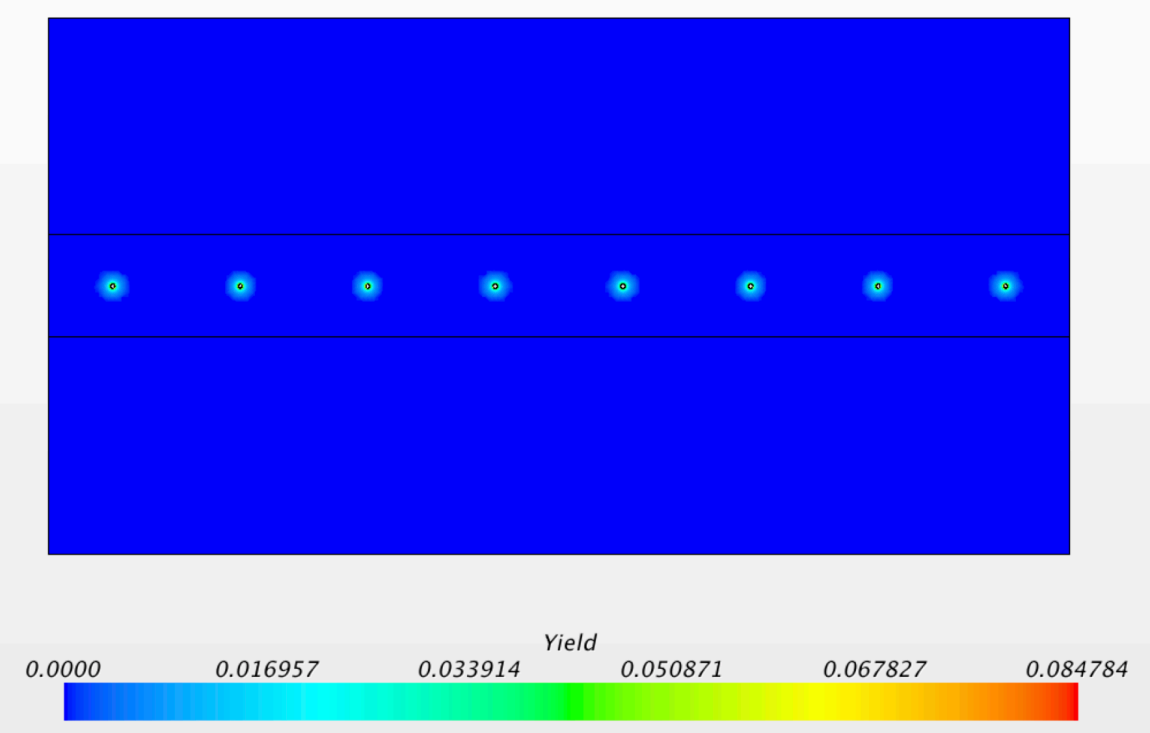


Figure 33. Front view of yield distribution for Yield 3 model with lower heater temperature of 675 K after 1,800 days of heating.

Figure 34 shows the mass of product (both liquid and gas) produced after heating the representative UCTT geometry for 1,800 days. As can be seen, the yield model used has a significant effect on the overall mass of product produced. Yield 1 (Y1) model predicts yields about an order of magnitude smaller than Yield 2 (Y2) model, whereas the base case, Yield 3 (Y3) model is in between the two previous models. The figure also reveals that the Yield 3 model with extended thickness of coal seam (Y3-Extended Domain) shows only a marginal improvement in mass production after 1,800 days when compared to Y3, the base case. Lastly, lowering the heating rate from 1073 K to 675 K has significant effects on the overall mass production of liquids and gases. The overall mass of product for the Yield 3 model with lower heater temperature (Y3-Lower Heat) after 1,800 days is about 14,000 kg, significantly lower than any other simulation.

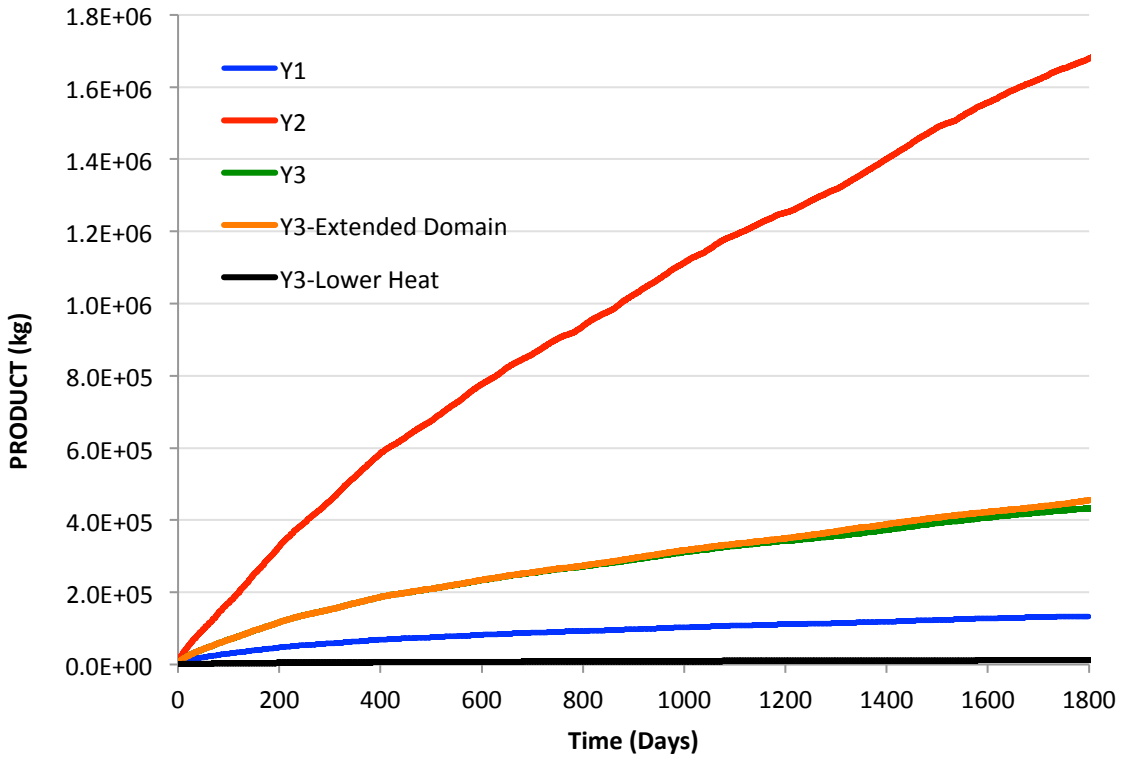


Figure 34. Variation in the mass of product for the five different simulations after 1,800 days of heating.

The mass of product plays a significant role in determining the overall NER for the process. These studies assumed that 1 kg of product mixture has energy equivalent of 30.4 MJ. Using this conversion and by tracking the amount of heat provided by the heaters, we can calculate the equivalent energy out versus the energy requirement in to determine the overall NER for the process. Figure 35 shows the NERs for the five simulations. As expected, the NER for the optimistic Yield 2 model (Y2) shows the greatest net energy return, while the Yield 3 model coupled with the lower heater temperature of 675 K (Y3-Lower Heat) shows the lowest NER. Based on these results, Yield models 2 and 3, as well as Yield model 3 with extended domain show NER values greater than four, i.e. for every unit of energy put into the formation as heat, four units of energy are produced. The NER of 18 for Yield 1 model coupled with heater

temperature of 1073 K is much greater than NER for any conventional source of oil and/or gas production currently available, and therefore is considered rather unrealistic. Yield 1 model and Yield 3 model coupled with lower heater temperature show NER values at or below one after 1,800 days of heating, deeming these scenarios economically unviable based on the assumptions going into the simulations.

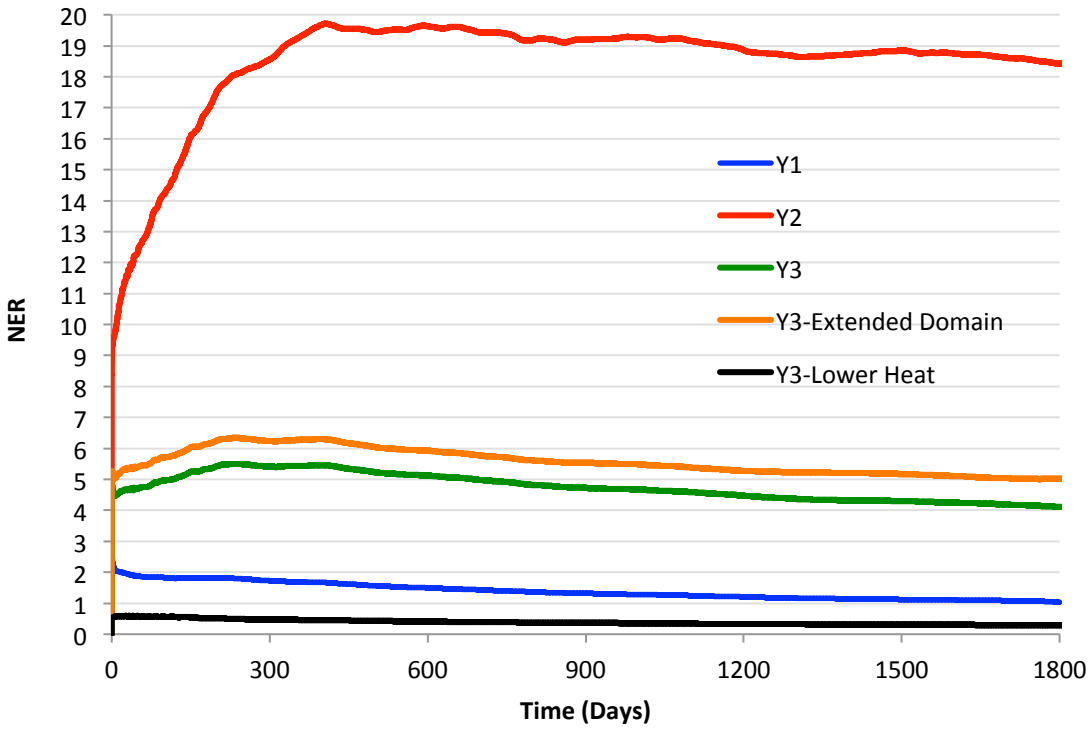


Figure 35. Calculated Net Energy Return for the five different simulations after 1,800 days of heating.

Another noticeable trend seen in Figure 35 is that for all simulations the NER decreases after about 400 days of heating. The NER continues to further decrease the longer the formation is heated. This declining trend in NER can be attributed to the increasing heat losses from the heater to the overburden and underburden as the heating continues. This is depicted in Figure 36, which shows the daily heat losses to the overburden and underburden relative to the heat input from the heaters. As can be seen from this figure, as the formation continues to be heated, the amount of heat going into the overburden and underburden continues to increase. The heat transferred to overburden and underburden is considered a heat loss since the heat leaves the coal seam and can no longer participate in producing tars or light gases. The largest heat loss occurs for the lower heater temperature simulation, even though simulations for Yield models 1, 2, and 3 are very similar. For these cases about 60 % of the daily heat provided by the heaters leaves the coal seam and enters the overburden and underburden. There is no heat leaving the coal seam for the extended coal seam domain and therefore the heat losses are zero after 1,800 days of heating.

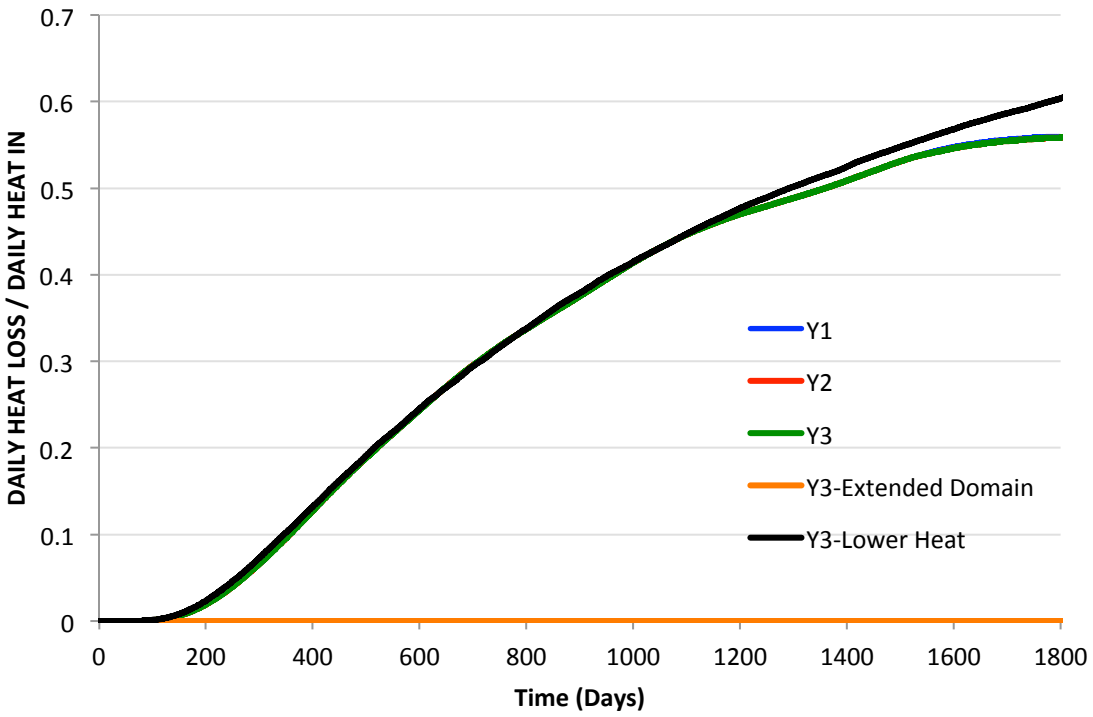


Figure 36. Daily heat loss to overburden and underburden versus daily heat input from heaters for all five scenarios.

Based on our results, the yield model as well as the heater temperature play the most crucial roles in determining the economic viability of a particular scenario. Currently most electric resistance heaters are able to sustain temperatures closer to the 675 K rather than the 1073 K as used for most of the simulations. Therefore, results presented in this report can yield artificially high NERs. Furthermore, the variability in production rates based on the different yield models as determined from the experimental runs, plays a crucial role in making a particular scenario economically viable. By varying the yield model alone, the production rates vary by an order of magnitude. Therefore, it is crucial to start with a realistic yield model to determine the overall process viability. Of course, results presented in this study are based on conductive-only simulations and do not include the many complexities that would naturally occur during an underground thermal treatment of coal. However, any assumptions made for these simulations were based on best estimates and approximations currently available.

## $CO_2$ storage studies

### Pyrolysis mass losses

Coals from the Carlinville mine in Utah, the Carlinville mine in Illinois, and the North Antelope mine in Wyoming were pyrolized in a tube furnace in an anoxic environment. The coals were heated to final

temperatures of 325, 450, or 600°C with heating rates of 10 or 0.1°C per minute. As part of the pyrolysis procedure, masses of the coals were recorded before and after each experiment.

The results for the mass losses for the coals can be found in Table 7. The results in Table 7 are reported on a dry basis as free (DAF) basis. Reporting values on a DAF basis was done to help with comparison, the North Antelope coal contained a lot more moisture compared to the Sufco and Carlinville coals.

Table 7. Percentage mass losses from pyrolysis. Results reported on a dry basis.

| Thermal Treatment | Skyline | Carlinville | North Antelope |
|---|---|---|---|
| 325 @10°C/min | 8.09 | 4.34 | 20.97 |
| 450 @10°C/min | 25.48 | 17.78 | 34.3 |
| 600 @10°C/min | 30.3 | 25.66 | 41.98 |
| 325 @0.1°C/min | 11.25 | 7.23 | 23.66 |
| 450 @0.1°C/min | 19.15 | 17.2 | 25.06 |
| 600 @0.1°C/min | 31.58 | 26.54 | 29.64 |

This study was not concerned with the either the kinetics of pyrolysis or the products; therefore proximate analysis of the pyrolysis products was not performed. Further, due to the large quantity of coal needed for isotherm measurements, setting up a sample loop to capture a representative sample would have proven technically troublesome. There is some existing literature pertaining to coal pyrolysis with slow heating rates (Solomon et al. 1993; Karanikas et al. 2004; Vinegar et al. 2004; Di Nola et al. 2010), and the experimental studies subtask also provide coal pyrolysis results.

Table 7 shows that the Carlinville coal had the least amount of mass loss while the North Antelope had the greatest. A general trend in the data can also be easily noticed; higher treatment temperatures resulted in larger mass loss. The effects of heating rate are not as conclusive. The Sufco and Carlinville coals, both bituminous, generally showed larger mass losses with slower heating rates, while the North Antelope coal (sub bituminous) showed more mass loss with faster heating rates. It is a possibility that the faster heating rate caused a quick buildup of pressure that may have blasted off small coal particles.

**Pore size distributions**

Pore size distributions were performed using a combination of two different methods. Density Functional Theory (DFT) (Lastoskie et al. 1993) was used to characterize micropores (<20Å), and Barrett-Joyner-Halenda (BJH) (Barrett et al. 1951) was used for pores larger than 20Å. The BJH analysis encompassed most of the mesopore range (20Å-500Å) as well as some of the larger pores in the macropore range (>500Å). Pore sizes were measured using a Micromeritics Tristar II using $CO_2$ as the adsorbate at 273.15K. Sohxlet extraction with acetone was employed to determine the effects of residual tars on the pores. Acetone is a mild solvent and was chosen because it is unlikely that it would damage the structure of the coal matrix.

There is a small gap in the data provided by the two methods. This discontinuity usually occurs between 20Å and 30Å, and it is easily recognized as a sudden dip in the pore size distributions within this range. With this in mind, it is important to interpret the area preceding the discontinuity independently from the area following the discontinuity. Furthermore, since the methods used for micropores and mesopores are different, there may be discrepancies in the estimated pore volumes and the true pore volumes. Pore volumes from DFT and BJH were plotted together to provide an *ab ovo* approach for pore sizes measureable using the Tristar II with $CO_2$. Pore size distributions were performed before and after high-pressure adsorption measurements; however there was little difference between the two measurements.

*Sufco coal*

The pore size distributions for the untreated and thermally treated Sufco coals can be found in Figure 37. Pore volumes increased with treatment temperature after 325°C. Like the surface area for the coals treated to 325°C being less than that of the fresh coal, there is a slight reduction in pore volumes from that of the unreacted coal over the entire range of pores measured. This reduction in pore volumes occurred regardless of heating rate. Coals treated to 450°C showed an increase in the mesopore ranges for both heating rates with a larger increase in mesopores. Coals treated to 450°C with a heating rate of 0.1°C/min showed little increase in micropores while the coal treated to the same temperature with a heating rate of 10°C/min showed a noticeable increase. Both coals treated to 600°C showed large increases over the entire range of measured pore sizes. The coal treated to 600°C with a heating rate of 10°C/min showed larger increases in the micro- and mesopore regions than the coal heated with a rate of 0.1°C/min.

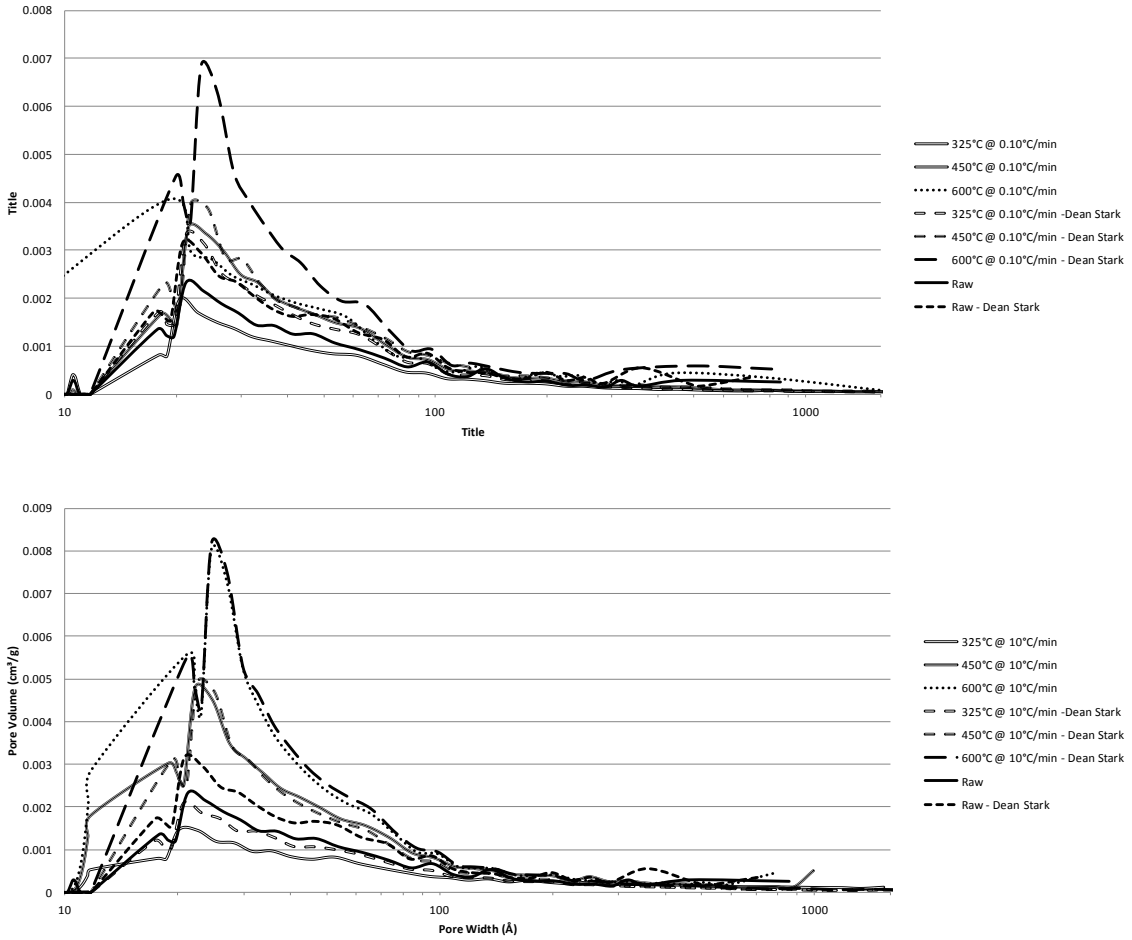


Figure 37. Pore-size distributions for the unreacted and the thermally treated Sufco coals, top 0.1°C/min and bottom 10°C/min. Solvent extraction (Dean-Stark) was used to determine effect of residual hydrocarbons on pore sizes.

Solvent extraction on the untreated and thermally treated Sufco coals showed interesting results with pore-size distributions. Sohxlet extraction on the untreated Sufco coal showed increases in both meso- and micropore volumes. The increase in pore volumes implies that some tar filled the pores. Solvent extraction on the coal treated to 325°C with a heating rate of 0.1°C/min showed increases in the mesopore range larger than that of the solvent-extracted untreated coal but showed little difference with respect to micropores. Extracted Sufco coal treated to 325°C with a heating rate of 10°C/min showed meso- and micropores volumes still less than that of the untreated coal. The fact that removing residual hydrocarbons did not increase the pore size distributions for this coal implies that another mechanism, such as plastic deformation, is responsible for this reduction.

Solvent extraction on the coal treated to 450°C with a heating rate of 0.1°C/min showed slight increases in both the micropore and mesopore ranges while extraction on the same coal treated to the same temperature with a heating rate of 10°C/min showed negligible change in the mesopore region and a

decrease in the micropore region. This difference demonstrates some of the competing kinetics occurring between plastic deformation and pore development in the coal matrix and remaining tars. The effects of plastic deformation at 450°C are overshadowed by pores created via pyrolysis. With the slow heating rate, it is likely that eluted tars begin filling pores slightly reducing their volume while with the faster heating rate, most of the tars in the mesopore region have completely volatilized but some tar remained creating abundances of micropores.

This idea of kinetic competition for pore development with Sufco coal is further justified after examination of the solvent-extracted coals treated to 600°C. With the coal treated to 600°C at 10°C/min, there is little change in the mesopore distribution but an increase in the micropore distribution; this is similar to the coal treated to 450°C with the same heating rate. However, regarding the coal treated to 600°C with a heating rate of 0.1°C/min, there is an increase in the micropores and a large decrease in the mesopores after solvent extraction meaning that some of the mesopores in this sample are in tars. The interpretation of the solvent extraction on the thermally treated Sufco coals is summarized in Table 8.

Table 8. Interpretation of pore size development of Sufco coals after solvent extraction.

| Thermal Treatment | Micropores | Mesopores |
|---|---|---|
| 325°C @ 0.1°C/min | plastic shrinking | plastic shrinking |
| 450°C @ 0.1°C/min | net increase / tar filling | net increase / tar filling |
| 600°C @ 0.1°C/min | net increase / tar filling | exist in tar |
| 325°C @ 10°C/min | plastic shrinking | plastic shrinking |
| 450°C @ 10°C/min | net increase / tar filling | net increase / no tar |
| 600°C @ 10°C/min | net increase / tar filling | net increase / no tar |

Sometimes an analogy with a common household item is useful in explaining an otherwise abstract concept. For coals undergoing slow pyrolysis, it is mentally beneficial to compare the process to something else that undergoes deformation when heated, cheese. Swiss cheese works well for this mental depiction as it has naturally occurring small and large pores to represent the initial pores in the coal. As the cheese is heated, it softens and some of the original pores are reduced in size or completely closed off; this is like heating the Sufco coal to 325°C. Once a certain temperature is reached, components volatilize creating internal pressure causing bubbles that eventually burst. If the heating rate is fast enough, some of these bubbles set but if the heating rate is slow, some of these bubbles are still subject to closure from plastic deformation. Oil that separated from the cheese collects on the surface and in the pores. Now imagining that this oil can dry out and by doing so creates even more pores; this is akin to pores developing in the residual tars of the coal only to have the porous media washed away with solvent extraction.

*Carlinville coal*

The pore size distributions on the Carlinville coals showed some major differences when compared to the Sufco coal. While the Sufco coal showed large increases in the range greater than 20Å, the Carlinville coal showed more changes in the micropore region. Pore size distributions for the untreated and thermally treated Carlinville coals can be found in the Appendix B. The shift between the largest pore

abundances between these two coals is not great and is likely the result of differences in the original coal matrix structure. With the unreacted Carlinville coal, the largest amount of pore volume occurs around 20Å with solvent extraction showing increases in both the micro- and mesopore regions. Like the Sufco coal, pore volumes tend to increase with treatment temperature. The Carlinville coal treated to 325°C with a heating rate of 0.1°C/minute had pore size distributions almost identical to the untreated coal even after solvent extraction implying that little physical change occurred in the coal structure. Carlinville coal treated to 325°C with a heating rate of 10°C/minute showed an increase in the high micropore/ low mesopore region with solvent extraction showing only slight differences. The coal treated to 450°C with a heating rate of 10°C/minute showed a shift into the mesopore region with the largest increase around 20Å. The increase in this coal remained after solvent extraction but shifted into the micropore region. The coal treated to 450°C with the slow heating rate had a large increase over the entire range of pore sizes after solvent extraction. Both coals treated to 600°C showed a significant increase across the entire pore distribution with solvent extraction increasing those pore volumes.

*North Antelope coal*

The North Antelope coal pore size distributions (Appendix C) shared a similar trend with the Carlinville and Sufco coals in that the pore volumes increased with the extent of thermal treatment and that the coals treated to a final temperature of 325°C showed similar or lesser pore volumes than the unreacted coal. This trend seems to be universal across all the coals and shows that at low pyrolysis temperatures pore changes are largely dominated by plastic deformation. When the unreacted coal was treated with acetone extraction, a large increase in the micropore region was observed implying that pre-existing hydrocarbons were blocking these pores. Solvent-treated coals heated to 325°C showed increases in the micro- and mesopore regions, but both were still less than the solvent extracted untreated coal. This lends credibility to the hypothesis of small pores swelling shut at lower treatment temperatures. The North Antelope coal treated to 450°C with the fast heating rate showed a net increase over that of the unreacted coal and coals treated to 325°C and solvent extraction caused little change in pore volumes.

The coal treated to 450°C with the slower heating rate also showed an increase in pore volumes but less than that of the coal treated with the faster heating rate, also there was more pore volume after solvent extraction. The trend of the coals treated to 450°C with the faster heating rate showing little change in pore volumes after solvent extraction occurs with all coals; also, the trend of coals treated to 450°C with the slower heating rate universally showing increases in pore volumes after solvent extraction. These trends occurring with coals treated to 450°C are results of competing pore-changing processes occurring near this temperature. At this temperature, the coal softens, and a combination of rapid expulsion of pyrolysis gases and explosive particle ejection are evident with fast heating rates. Softening and expansion of pores is seen with the slower heating rate, but these pores soon filled with produced tars only to be revealed with solvent extraction.

Although the trends at 450°C seem transient across all coal types in these experiments, the results of the pore size distributions on coals treated to 600°C seem more coal-type dependent. The North Antelope coals treated to 600°C showed large increases in the micropore and mesopore regions, but solvent extraction proved that a significant portion of these increases were in residual hydrocarbons. While this is

similar to the Carlinville coals, it differs from the Sufco coal where pores obstructed by residual hydrocarbons.

There are some common trends between changes in pore size distributions with certain treatment temperatures/rates; there are also some discrepancies with other temperatures and rates. These discrepancies seem related to the coals used in these experiments suggesting that in an actual implementation of UCTT, performing measurements on the target coal to better estimate pore sizes.

**Adsorption isotherms**

High-pressure adsorption measurements were performed on the equipment similar to that used by Mavor et al. (1990) located at TerraTek (a Schlumberger company) in Salt Lake City, UT. Isotherm measurements were performed at temperatures of 50 or 70°C with $CH_4$ or $CO_2$. Results of the isotherm measurements were fitted to the Langmuir equation fully knowing that the assumptions of the Langmuir do not accurately describe the physical nature of the adsorbed phase; the Langmuir equation, however, is often used in industry to describe adsorption of coal and shale. It is often used to model adsorption in reservoir simulators and decently fits adsorption data. In this study, the results of 84 individual isotherms were presented with each individual isotherm requiring about one week to process. Isotherms were plotted with the various terminal treatment temperatures with the heating rate at which they were treated alongside the isotherm of the untreated coal. It was hypothesized that there is a relationship between the adsorptive capacities of the coals and the thermal treatment temperature. This relationship was further hypothesized to be related to the pore size distributions in the coal. Like the pore size distributions, there were some unilaterally recognized trends in the isotherm data. In this section, an attempt was made to develop a relationship between adsorptive capacity and coals thermally treated with slow heating rates.

*Sufco coal*

Like the surface area measurements and pore size distributions, the high-pressure isotherm measurements on the Sufco coal showed trends dependent on the treatment temperature but not so much with heating rate. For each of the coals used in this study, there are eight unique plots. Each plot shows the three coal samples treated at a given heating rate plus the untreated coal for comparison. The results of the adsorption isotherm measurements for the fresh and thermally treated Sufco coal (heat rate of 0.1°C/minute) can be found in Figure 38; adsorption isotherms for the Sufco coal treated with a heating rate of 10°C/minute can be found in Figure 39.

High-pressure isotherms for the thermally treated coals showed similar trends to those observed with the pore size distributions and surface area measurements. Isotherms on coals treated to 325°C showed less adsorptive capacity than the fresh coals, and the capacity of the coals increased with treatment temperature. The adsorptive capacity of the coals increased with treatment temperature. The effect of heating rate on adsorptive capacity is less pronounced than the effect of pore size distributions. As expected, the adsorptive capacity for $CO_2$ exceeded that of $CH_4$, and the volume adsorbed decreased with measurement temperature.

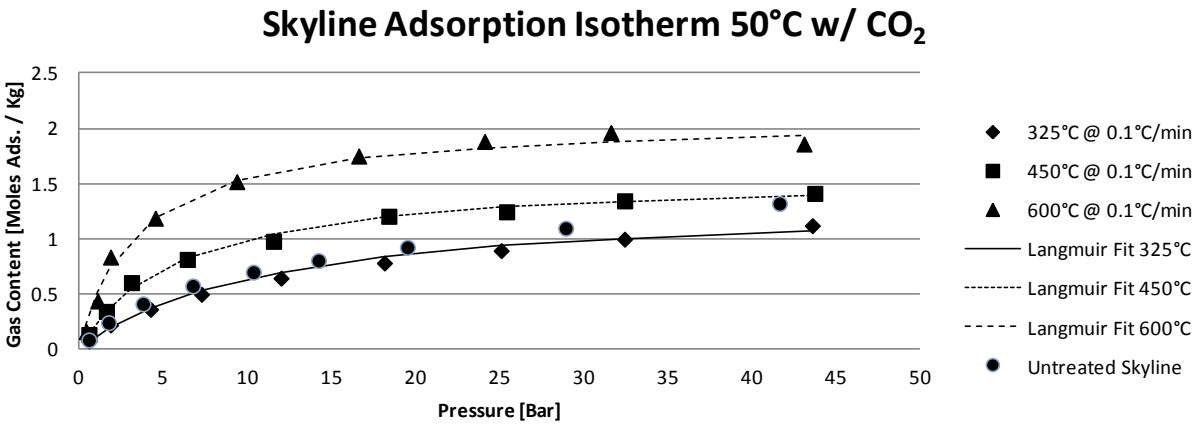
Skyline Adsorption Isotherm 50°C w/ CO2
Gas Content [Moles Ads. / Kg]
Pressure [Bar]
325°C @ 0.1°C/min
450°C @ 0.1°C/min
600°C @ 0.1°C/min
Langmuir Fit 325°C
Langmuir Fit 450°C
Langmuir Fit 600°C
Untreated Skyline

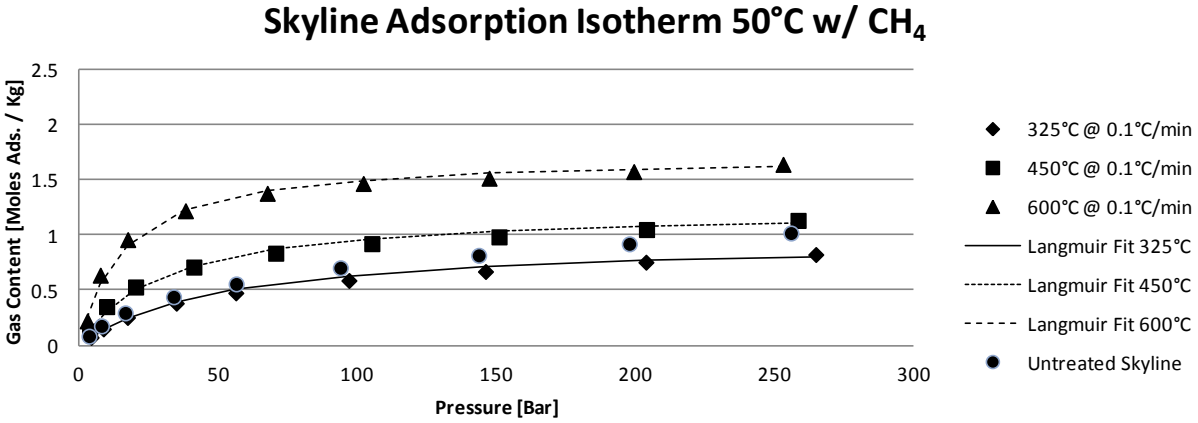
Skyline Adsorption Isotherm 50°C w/ CH4
Gas Content [Moles Ads. / Kg]
Pressure [Bar]
325°C @ 0.1°C/min
450°C @ 0.1°C/min
600°C @ 0.1°C/min
Langmuir Fit 325°C
Langmuir Fit 450°C
Langmuir Fit 600°C
Untreated Skyline

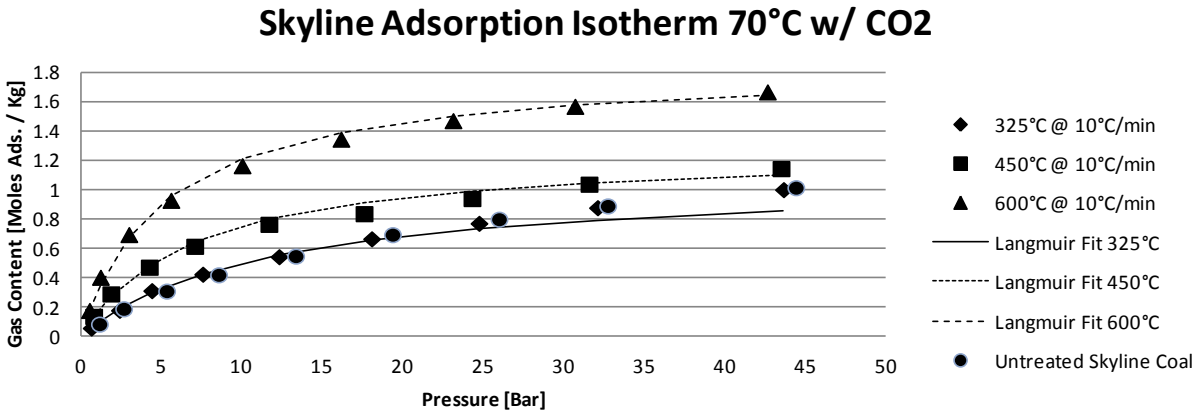
Skyline Adsorption Isotherm 70°C w/ CO2
Gas Content [Moles Ads. / Kg]
Pressure [Bar]
325°C @ 10°C/min
450°C @ 10°C/min
600°C @ 10°C/min
Langmuir Fit 325°C
Langmuir Fit 450°C
Langmuir Fit 600°C
Untreated Skyline Coal

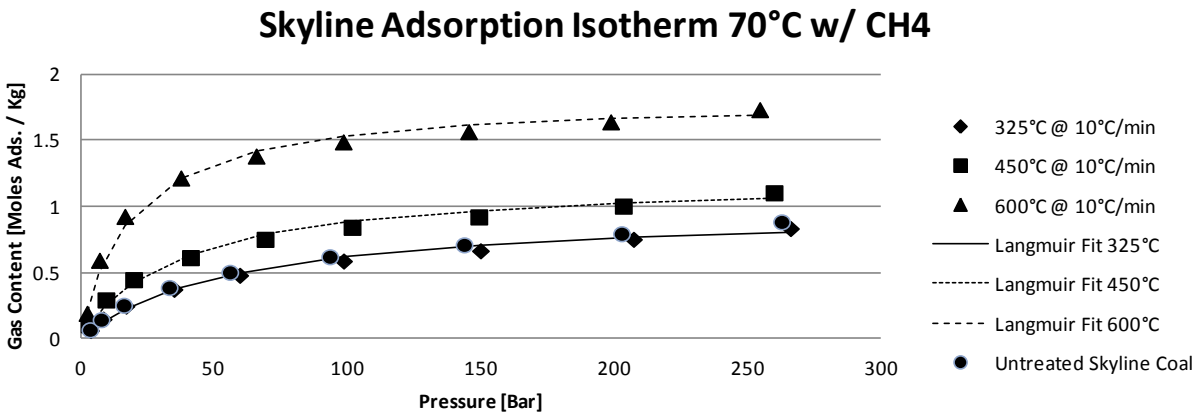


Figure 38. Example of high-pressure adsorption isotherms for thermally treated Sufco coal treated with a heating rate of 0.1°C/minute. The figures say Sufco coal, but it was later confirmed to be Sufco coal. Adsorption values reported in moles of adsorptive per kilogram of coal (dry basis).

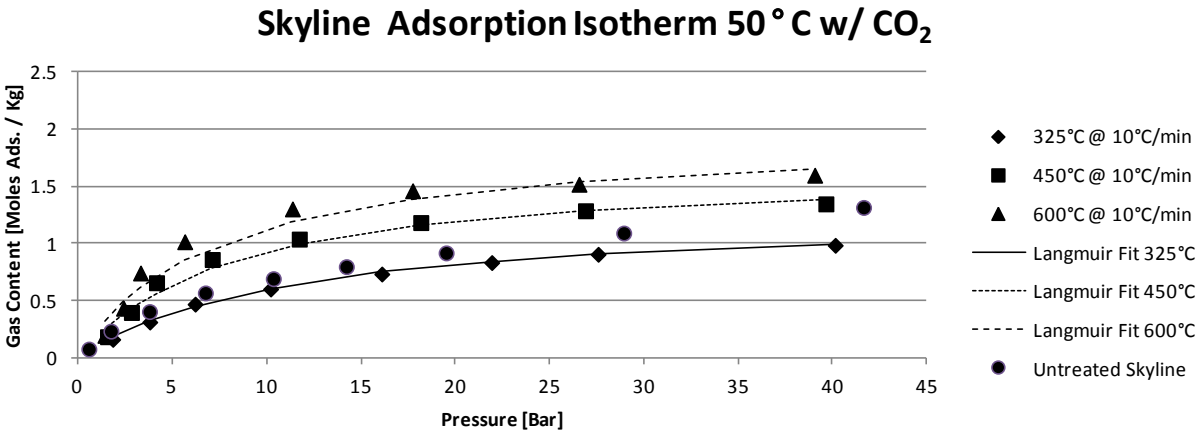


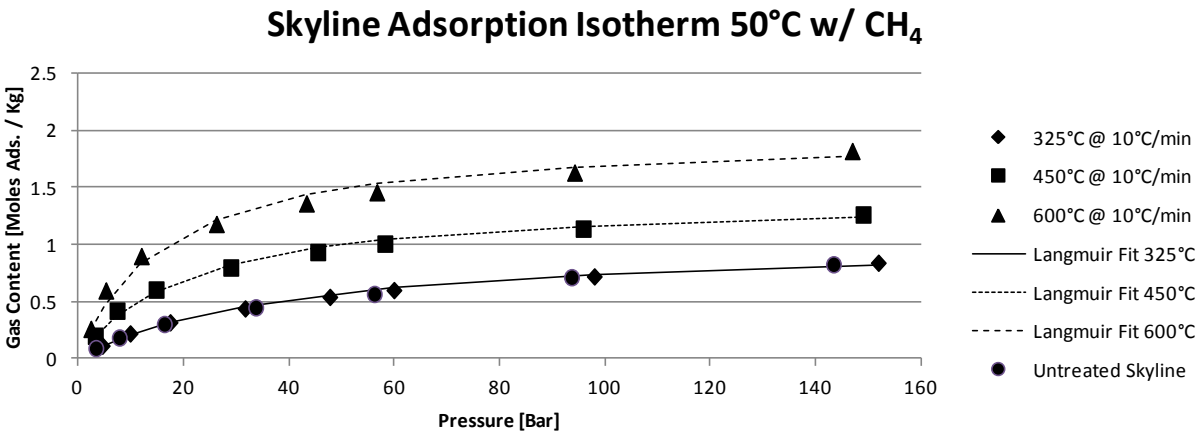

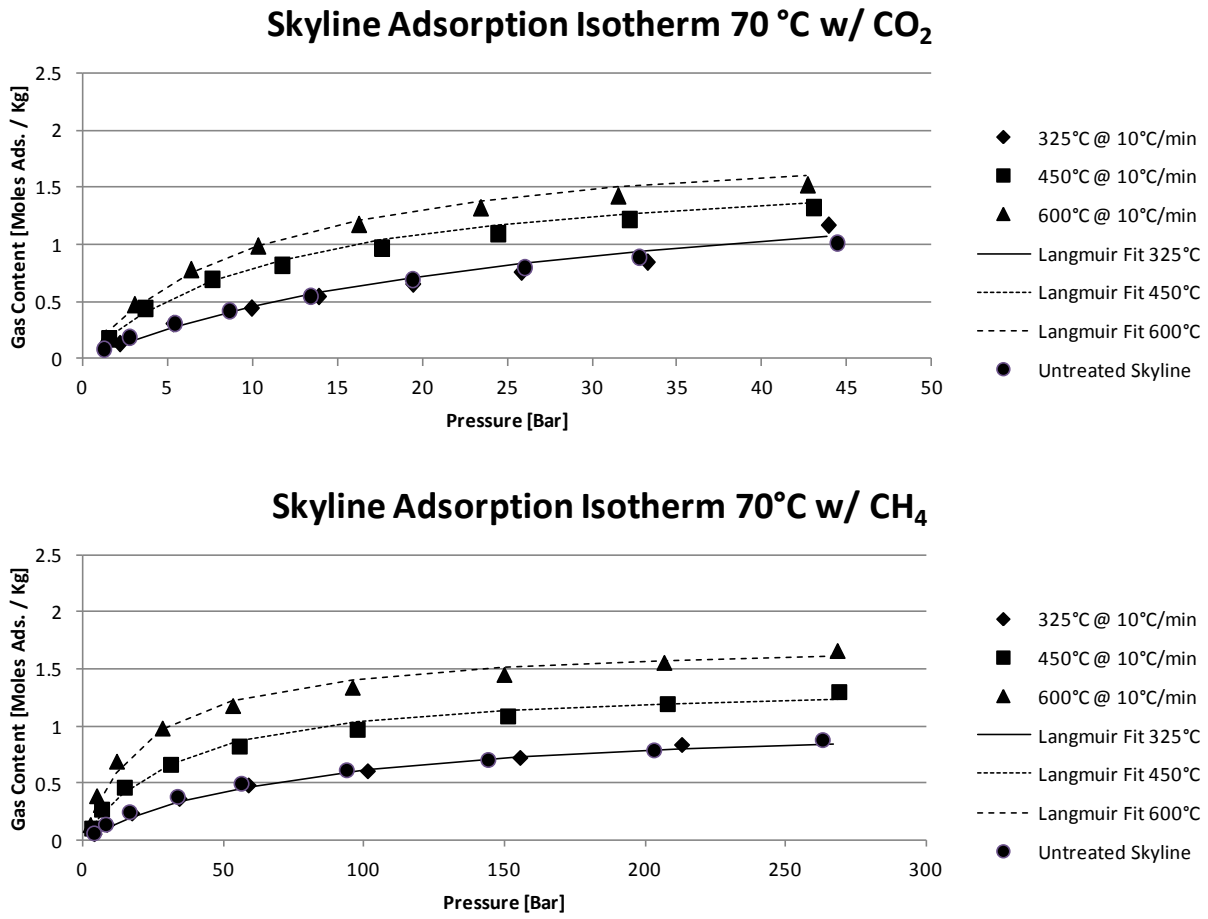


Figure 39. Adsorption isotherms on unreacted and thermally treated Sufco coal. The heating rate for treated coals in this figure was 10°C/minute. The figures say Skyline coal, but it was later confirmed to be Sufco coal. These coals showed trends similar to Sufco coals treated with the slower heating rate.

Adsorption values were fitted to the Langmuir adsorption equation, which provides theoretical maximum adsorptive capacities and curvature of the isotherm. The Langmuir equation defines the adsorbed phase as a single layer; with coals this is not the case. The Langmuir equation, however, does fit the adsorption data with a good degree of agreement and is commonly used to model adsorption on coals. The $R^2$ value from the linear regression fitting data to the Langmuir equation was at least 0.97 and very commonly 0.99 or better. Langmuir fitting parameters treated coals can be found in Table 9 and Table 10; in these tables the units of $V\infty$ is in moles adsorbed per kilogram, $\beta$ is in 1/bar.

Table 9. Langmuir fitting parameters for isotherms on coals thermally treated with a 10°C/minute heating rate. V∞ is in moles adsorbed per kilogram, β is in 1/bar.

| Coal | Langmuir Fit | $CH_4$ @ 50°C | $CH_4$ @ 70°C | $CO_2$ @ 50°C | $CO_2$ @ 70°C |
|---|---|---|---|---|---|
| Skyline | V∞ | 1.174 | 0.885 | 1.590 | 1.213 |
| | β | 1.9716E-04 | 2.4246E-04 | 8.6001E-04 | 6.4895E-04 |
| 325@0.1 | V∞ | 0.952 | 0.964 | 1.353 | 1.076 |
| | β | 2.0204E-04 | 1.8033E-04 | 8.7402E-04 | 8.7112E-04 |
| 450@0.1 | V∞ | 1.224 | 1.208 | 1.584 | 1.273 |
| | β | 3.4853E-04 | 2.6775E-04 | 1.6839E-03 | 1.4398E-03 |
| 600@0.1 | V∞ | 1.720 | 1.818 | 2.081 | 1.841 |
| | β | 6.5414E-04 | 5.3187E-04 | 2.9443E-03 | 1.9048E-03 |

Table 10. Langmuir fitting parameters for coals treated with a 0.1°C/minute heating rate. V∞ is in moles adsorbed per kilogram, β is in 1/bar.

| Coal | Langmuir Fit | $CH_4$ @ 50°C | $CH_4$ @ 70°C | $CO_2$ @ 50°C | $CO_2$ @ 70°C |
|---|---|---|---|---|---|
| Skyline | V∞ | 1.174 | 0.885 | 1.590 | 1.213 |
| | β | 1.972E-02 | 2.425E-02 | 8.600E-02 | 6.490E-02 |
| 325@10 | V∞ | 1.034 | 1.072 | 1.267 | 1.742 |
| | β | 2.473E-02 | 1.341E-02 | 8.938E-02 | 3.561E-02 |
| 450@10 | V∞ | 1.404 | 1.393 | 1.666 | 1.742 |
| | β | 4.884E-02 | 2.952E-02 | 1.237E-01 | 8.366E-02 |
| 600@10 | V∞ | 1.957 | 1.742 | 1.947 | 1.990 |
| | β | 6.289E-02 | 4.434E-02 | 1.392E-01 | 9.679E-02 |

*Carlinville coal*

The isotherms measured on the Carlinville coals showed trends very similar to those shown by the Sufco coals. The measured values of the adsorbed gas on the Carlinville coals were similar in magnitude to the Sufco coals. These isotherm plots for the Carlinville coals are in Appendix D. Like the Sufco coals, the Carlinville coals treated to 325°C showed capacities rarely greater than unreacted coal. Also like the Sufco coal, the Carlinville coals showed increases in capacity with the extent of thermal treatment temperature. And as expected, the capacity for $CO_2$ exceeded that of methane, and adsorptive capacity decreased with measurement temperature. Langmuir equation fitting parameters for the Carlinville coal can also be found in Appendix D.

*North Antelope coal*

Isotherms on the unreacted and thermally treated North Antelope coals showed trends identical to those of the Sufco and Carlinville coals. Coals treated to 325°C showed reduced capacity compared to the unreacted coal, and adsorptive capacity increased with final treatment temperature. Also, like the previous coals, the North Antelope coal showed little difference in capacity with either heating rate. North Antelope isotherms and Langmuir fitting parameters can be found in Appendix E.

*Correlations with pore size distributions*

One of the main hypotheses of this study is that a relationship exists between the final treatment temperature and adsorptive capacity; a relationship which is bridged through the pore size distributions of the coals. Throughout this work, similar trends were noticed with several different analytical techniques. For example, the Brunauer-Emmett-Teller (BET) surface area measurements showed increases with thermal treatment temperature, and the surface areas of the coals treated to 325°C were less than those of the unreacted coals. Pore size distributions showed increasing abundances of small pores with treatment temperature, and coals treated to the lowest temperature showed pore volumes less than those of the unreacted coals. Trends were related to the pore size distributions because the pore size distributions (PSDs) are the most encompassing characteristic of the coal surface. PSDs account for small pores where capillary condensation can occur affecting the adsorptive capacity. They also account for the surface area of small pores affecting overall surface area and the abundance of large pores, which affects permeability.

Maximum theoretical adsorptive capacities from the Langmuir equation were plotted against the measured pore volumes in the either the micropore or mesopore range. If pore condensation is prolific in high-pressure measurements, then the relationship would be a simple volume to volume comparison. Since determining the fraction of pores that were filled via pore condensation in the high-pressure measurements was not done, it is difficult to assume that all pores are filled by this mechanism.

The Sufco coals showed a definite relationship between adsorptive capacity and meso- micropores. This relationship held true for both $CO_2$ and $CH_4$ with both measurement temperatures. The relationship between adsorptive capacity and mesopore abundance was stronger for the Sufco coals than with the micropore volumes. The relationship between pores and capacity for $CO_2$ on Sufco coals can be found in Figure 40. Little relationship between pores and adsorption was found for the Carlinville coals. North Antelope coals, like the Sufco samples, also showed relationships between adsorptive capacity and micro to mesopores. However, unlike the Sufco coals, the relationships of either pore types to adsorptive capacity were nearly equal.

It is generally accepted that both mesopores and micropores attribute to adsorption. From this analysis, adsorption in thermally treated coals showed more a dependence on mesopores, but the contribution of the micropores should not be neglected. This work indicates that it may be possible to estimate the adsorptive capacity of a thermally treated coal seam with only a few laboratory isotherm measurements. There is also a cost and time benefit to these analysis. Before, if one wanted to thoroughly model gas potential or storage capacity of a thermally treated coal seam, they would have to perform a multitude of isotherm measurements. Adding the effects of treatment temperature gradients in a coal seam further

necessitates the need for more isotherm measurements by adding another degree of complexity. Now only a few isotherm measurements need to be performed and correlated to DFT/BJH pore size distributions. From the correlation between pyrolized coal and pore size distributions, adsorptive potential could be inferred from pore size distributions. For comparison, PSDs are an order of magnitude less expensive and require only a day to perform compared to weeks for full isotherms.

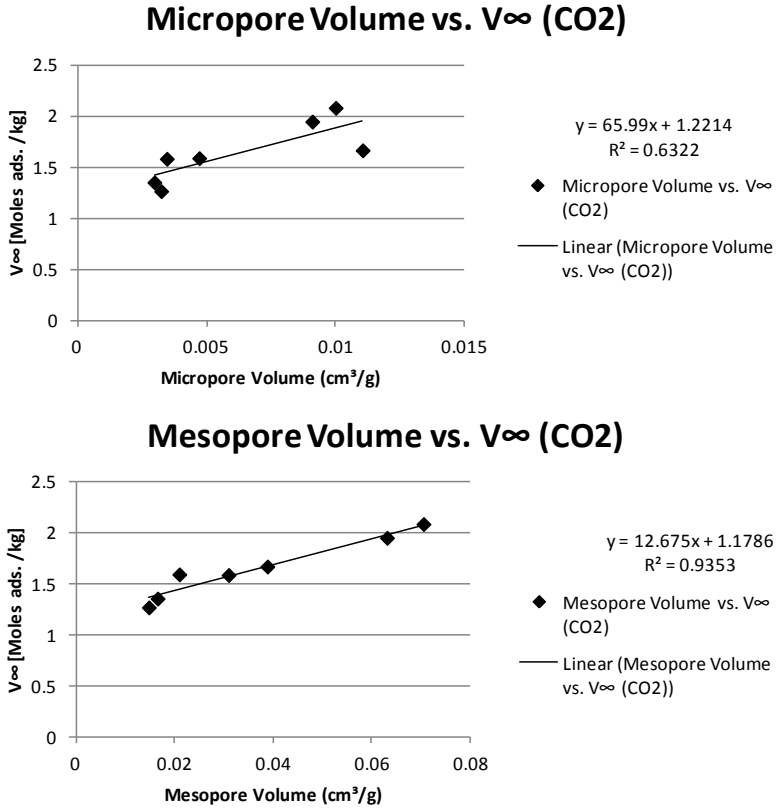


Figure 40. Relationships between maximum theoretical adsorptive capacity and the amounts of mesopores and micropores for the Sufco coal. The relationships presented in this figure were for $CO_2$ isotherms measured at 50°C; however, the trends held for other temperatures and for measurements using methane.

**Adsorption simulation studies**

Injection recovery simulations were done on a 100x100x9 m domain for Sufco coals treated to 325, 450, and 600°C with a heating rate of 0.1°C/minute. The values for adsorptive capacity came from experimental results. Multicomponent adsorption was modeled using the extended Langmuir equation. For the first 60 days of these simulations, methane was produced without the injection of $CO_2$. After 60 days, $CO_2$ was injected at a rate of 6000 $m^3$/day to displace the adsorbed methane in a process very similar to enhanced coal-bed methane. Carbon dioxide was injected until the 365$^{th}$ day, the end of the simulation. The results of the Sufco injection simulations can be found in Figure 41.

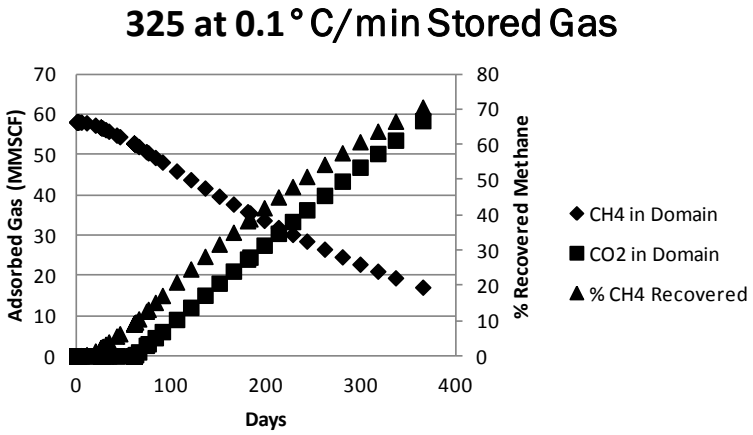


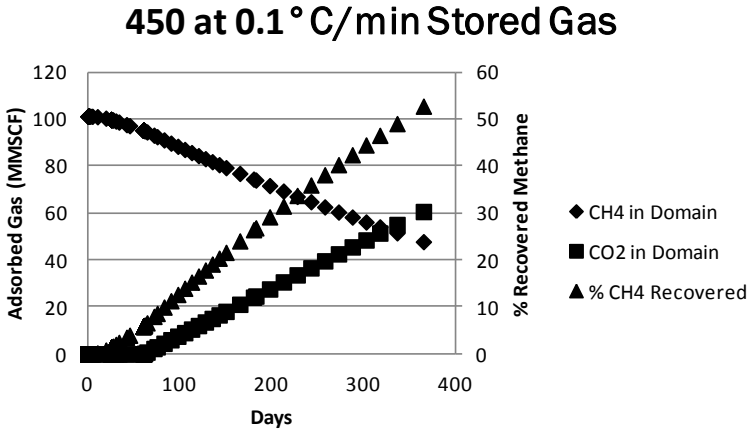

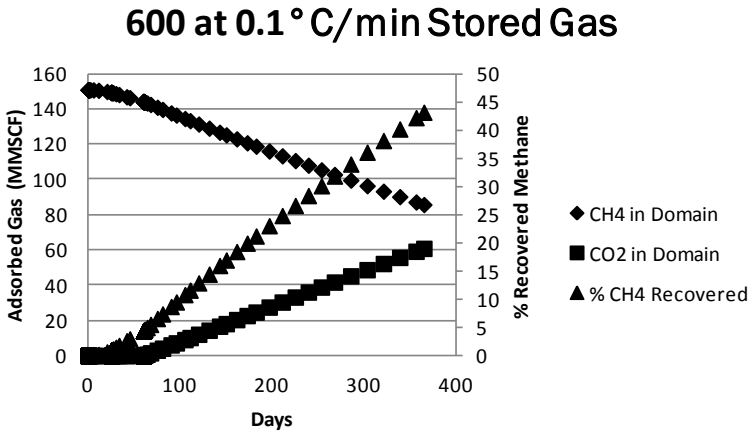


Figure 41. Domain gas content for injection / recovery simulations experimentally determined adsorption parameters. Values used were for Sufco coals treated with a heating rate of 0.1°C/minute. The trends in this figure were also seen with simulations for the other coals.

Figure 41 shows that the coal treated to the higher temperature has larger amount of initial methane and at the one year mark only about 43% initial methane recovery. Although the recovery percentage for the 600°C simulation is less than the others in Figure 41, the actual volume of methane recovered is greater for the 600°C simulation than the others. Since $CO_2$ was injected at the same rate for each simulation the amount of $CO_2$ stored in the formation was similar for each simulation.

**CONCLUSIONS**

*Experimental.* The experimental results indicate that yield is a function of temperature, with higher temperatures producing higher yields in the range of 20 – 28%. Despite the large difference in scale, the FBR and RBR yield and composition results agree reasonably well. The effect of pressure was not as pronounced as the effect of temperature, and the results were somewhat inconclusive. The effect of coal particle size on yield appeared to be limited, which may be due to the difference in coal particle size (roughly a 2.5" cube versus a 4 – 5" cube). The predominant gas-phase products from the UCTT reactor were methane and $CO_2$, and the liquid products were crude-oil like although they tended to exhibit more reactivity and double bonding than a typical crude.

*Simulation.* The evaluation of convective channels revealed the importance of convective channels for faster and more uniform heat distribution. The investigators also modeled heat transfer through a coal seam and evaluated various yield models based on experimental studies, as well as various seam thicknesses and heater temperatures. These studies suggested the importance of developing an accurate yield model for the low temperatures. Although numerous yield models exist, these are designed for the high temperatures and high heating rates associated with pulverized coal combustion, not the low temperatures present in a UCTT process.

*$CO_2$ storage*. Like other *in-situ* process, determining the amount of $CO_2$ that can be sequestered and the injection/recovery scheme relies on computational reservoir modeling, which relies on adsorption isotherms and permeability measurements to model $CO_2$ injections into coal seams. This work sought out to determine adsorption isotherms for both methane and carbon dioxide on three different coal samples heated with slow heating rates. Permeabilities of treated coals were also determined.

Preliminary characterization of the porous structure led to three questions. First, what contribution do residual hydrocarbons have on the porous structure? Results of the solvent extraction showed reduced surface areas for the coals treated to the lowest temperature. They also revealed that the reduction in pore volumes was due to a combination of residuals blocking pores and plastic deformation collapsing pores. Coals treated to higher temperatures showed evidence that a portion of the developed surface area attributable to hydrocarbon residuals. Coals that were treated to 450°C with a heating rate of 10°C/minute showed little influence of residual tars while coals treated to the same temperature at 0.1°C/minute showed increases in pore volume after solvent extraction. This means that for the 450°C samples treated with the slow heating rate tars were blocking access to some of the pores.

Second can properties of coals be related to treatment temperature or heating rate through a single measurement? All coals treated to a final treatment temperature of 325°C showed lesser or similar surface areas to the unreacted coals. The surface areas of the coals increased with the final treatment temperature but there was little relationship with the heating rate. Simulation results showed that coals treated to the highest temperature had the largest amounts of initial methane and the best methane recovery.

Third what porous regime, mesopore or micropore, has the largest effect on adsorption on thermally treated coals? Like the surface-area measurements, the pore volumes for coals treated to 325°C were less than those of the unheated coals. Mesopore and micropore volumes tended to increase with increasing treatment temperature. Coals treated to 600°C showed the largest increase in pore volumes. Surface area and pore size distributions were performed before and after high-pressure isotherm experiments, and the results showed that thermally treated coals exhibited little to no change after exposure.

High-pressure adsorption isotherms were performed volumetrically on the coals using methane and carbon dioxide. Coals treated to 325°C showed reduced capacity when compared to the untreated coals. In addition, adsorptive capacity generally increased with treatment temperature. The effect of heating rate was not obvious with the high-pressure adsorption measurements. Correlations between micropores or mesopores and adsorptive capacity showed strong relationships for the Sufco and North Antelope coals. The Sufco coals showed a stronger correlation with mesopores while the relationship was equally significant for meso- and micropores on the North Antelope coals. Correlations between adsorption and pores were similar with different analysis gases and different isotherm temperatures.

The pore size distribution measurements provided the best predictor of adsorption capacity and other measurements. Using pore size distributions indirectly accounts for the surface area contribution of pores, adsorption in pores, and transport through larger pores.

The observed trends were consistent for the three coals tested.

This work shows the importance of understanding the pore structure of thermally treated coals as it pertains to UCTT. In the past, with ECBM operations, multitudes of high-pressure isotherms were required to characterize the reservoir. Now, at least with UCTT, it may be possible to develop correlations between just a few high pressure isotherm measurements and pore size distributions and from this use the pore sizes to estimate the adsorptive capacity.

## REFERENCES


Barrett, E. P.; Joyner, L. G.; Halenda, P. P. The determination of pore volume and area distributions in porous substances. I. Computations from nitrogen isotherms. *J. Am. Chem. Soc.* 1951, 73(1), 373-380.

Beychok, M. 2011. Petroleum crude oil. *The Encyclopedia of Earth.* [Online] http://www.eoearth.org/.

British Petroleum (BP), June 2012. Statistical Review of World Energy 2012; http://www.bp.com (accessed November 28, 2013).

Di Nola, G.; De Jong, W.; Spliethoff, H. TG-FTIR characterization of coal and biomass single fuels and blends under slow heating rate conditions: partitioning of the fuel-bound nitrogen. *Fuel Process. Technol.* 2010, 91(1), 103-115.

Keller, J.; Staudt, R. *Gas Adsorption Equilibria*. 2005. New York: Springer.

Lastoskie, C.; Gubbins, K. E.; Quirke, N. Pore size distribution analysis of microporous carbons: a density functional theory approach. *J. Phys. Chem.* 1993, 97(18), 4786-4796.

Maroto-Valer, M. M.; Tang, Z.; Zhang, Y. CO2 capture by activated and impregnated anthracites. *Fuel Process. Technol.* 2005, 86(14–15), 1487-1502.

Mavor, M.J.; Owen, L.B.; Pratt, T.J. Measurement and evaluation of coal sorption isotherm data. Society of Petroleum Engineers Annual Technical Conference and Exhibition. New Orleans, LA, USA, 157-170, 1990.

Solomon, P.; Fletcher, T.; Pugmire, R. Progress in coal pyrolysis. *Fuel.* 1993, 72(5), 587-597.

US Energy Information Administration, 2012a. Recoverable Coal Reserves; http://www.eia.gov/coal/data.cfm#reserves (accessed November 28, 2013).

US Energy Information Administration, 2012b. Effect of Increased Natural Gas Exports on Domestic Energy Markets; http://www.eia.gov/analysis/requests/fe/pdf/fe_lng.pdf (accessed December 6, 2012).

Vinegar, H. J.; Wellington, S. L. et al. In situ thermal processing of a coal formation using a relatively slow heating rate. US6758268 B2, July 6, 2004.

## APPENDIX A. THERMOCOUPLE LOCATIONS IN THE RBR

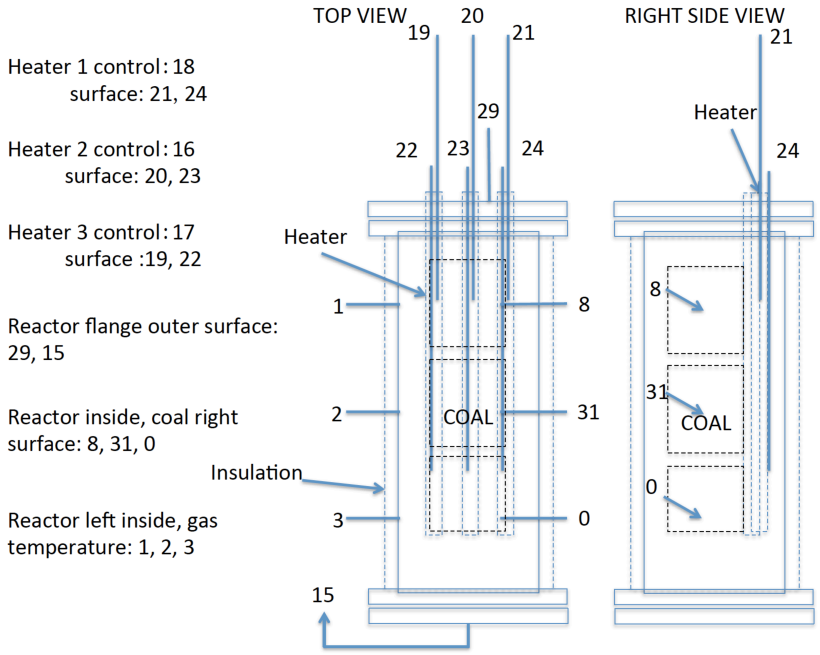


Figure A-1. Typical thermocouple locations for RBR experiments.

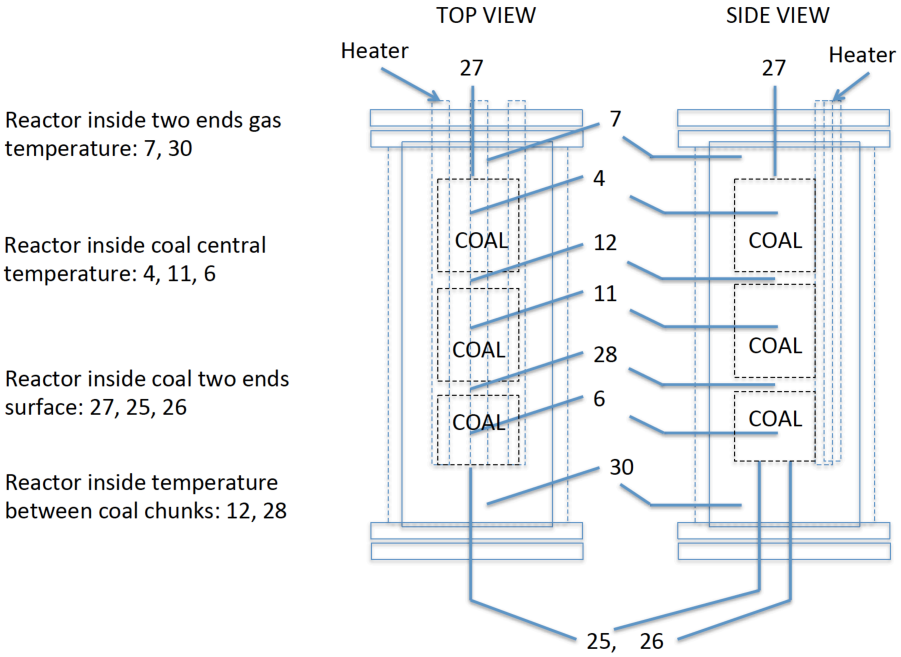


Figure A-2. Typical thermocouple locations for RBR experiments, continued.

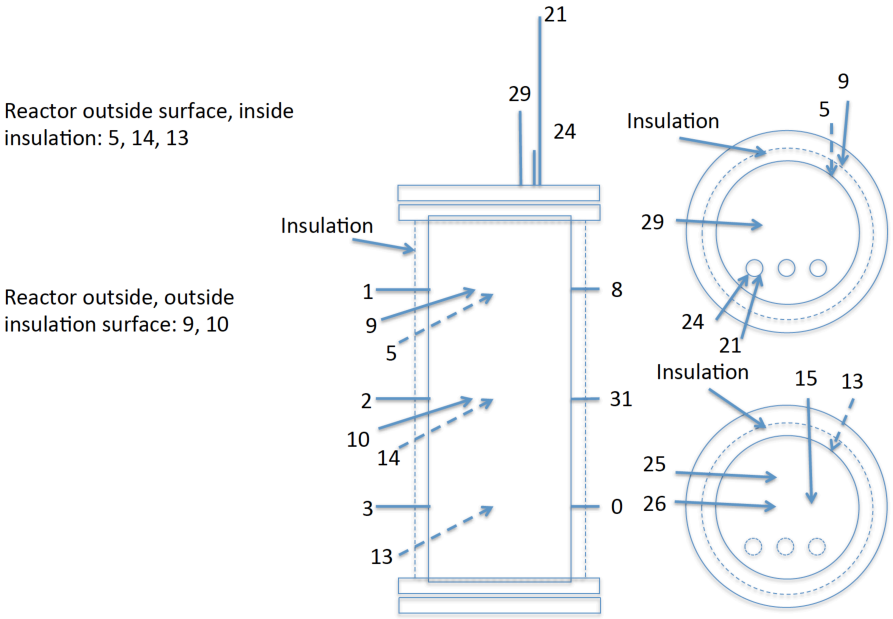


Figure A-3. Typical RBR thermocouple locations.

## APPENDIX B. CARLINVILLE COAL PORE SIZE DISTRIBUTIONS

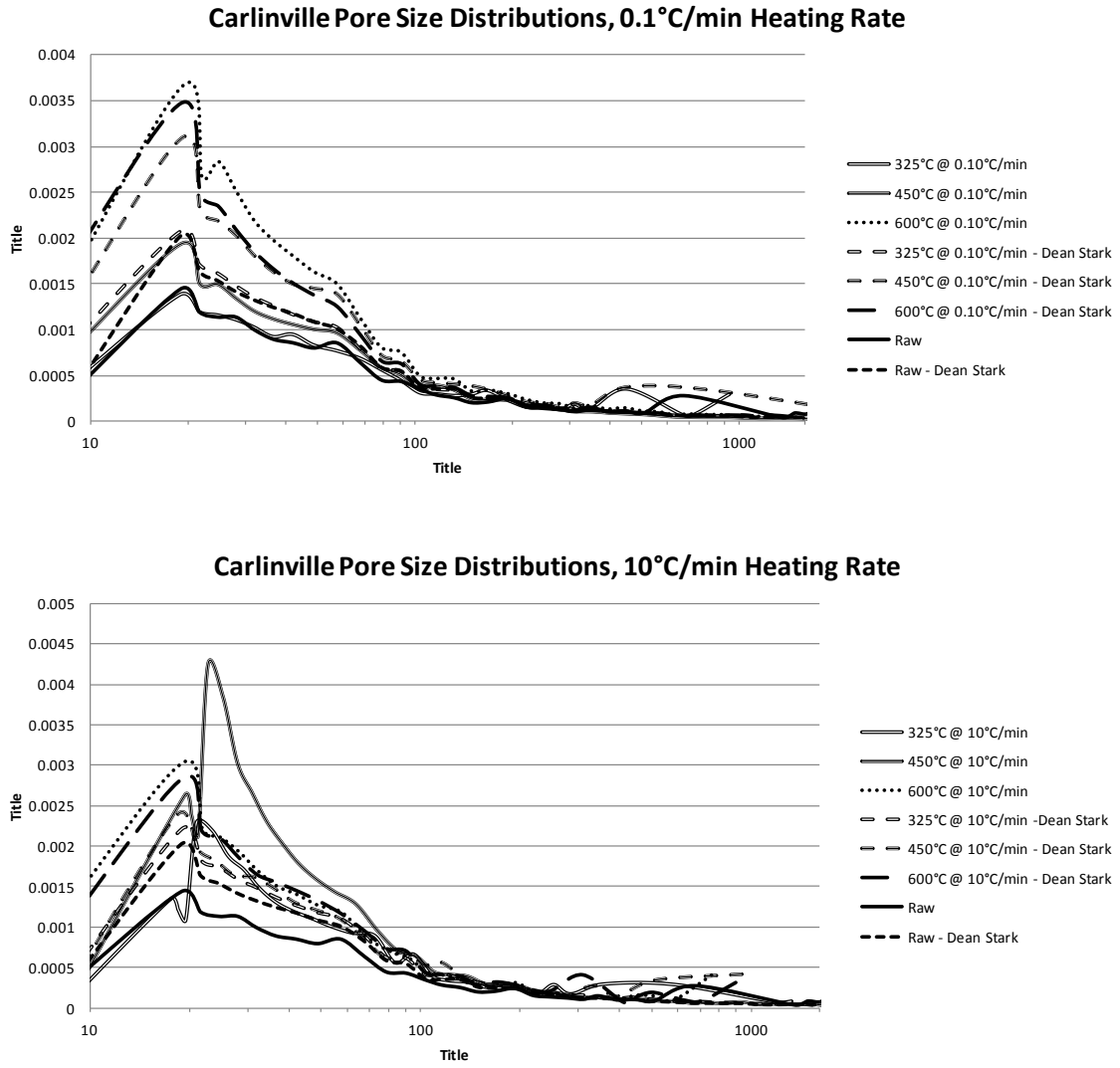


Figure B-1. Pore size distributions for the unreacted and the thermally treated Carlinville coals. Solvent extraction (Dean-Stark) was used to determine effect of residual hydrocarbons on pore sizes.

## APPENDIX C. NORTH ANTELOPE PORE SIZE DISTRIBUTIONS

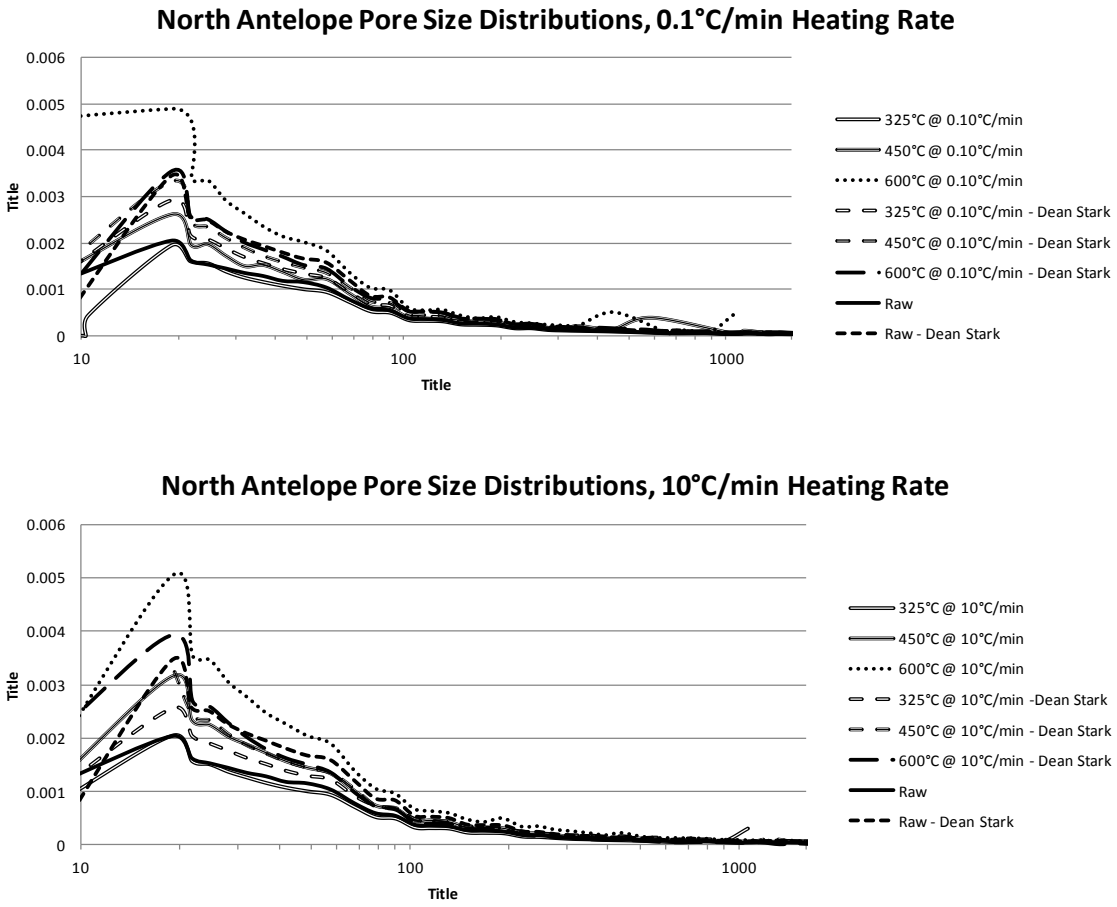


Figure C-1. Pore size distributions for the unreacted and the thermally treated North Antelope coals. Solvent extraction (Dean-Stark) was used to determine effect of residual hydrocarbons on pore sizes.

## APPENDIX D. CARLINVILLE ADSORPTION ISOTHERMS

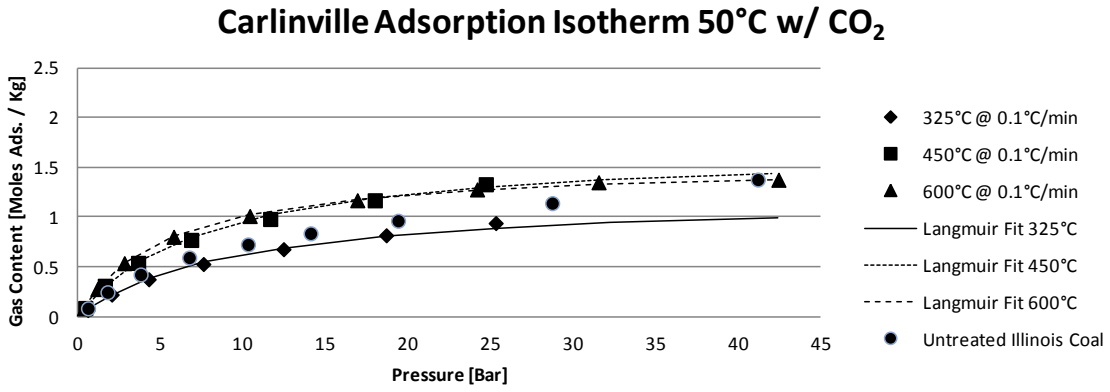


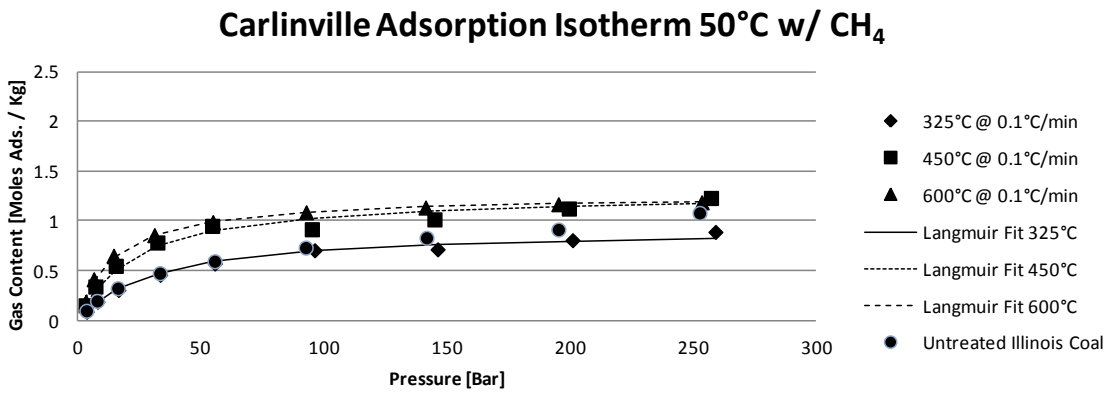


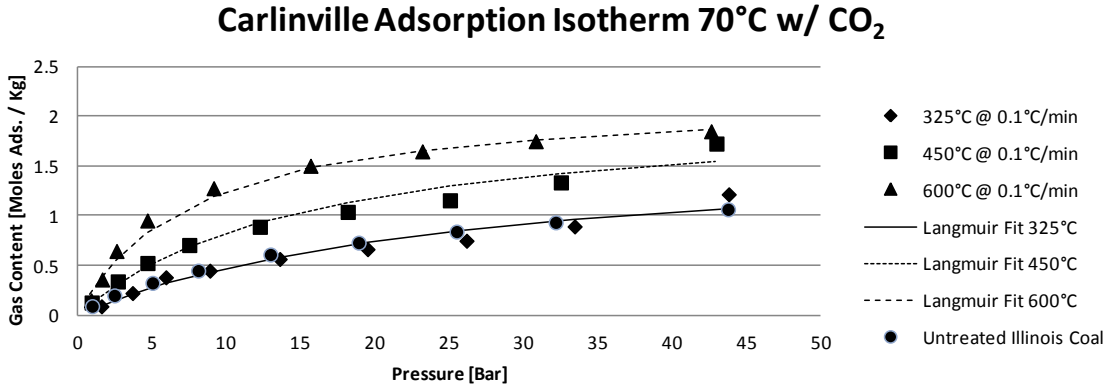

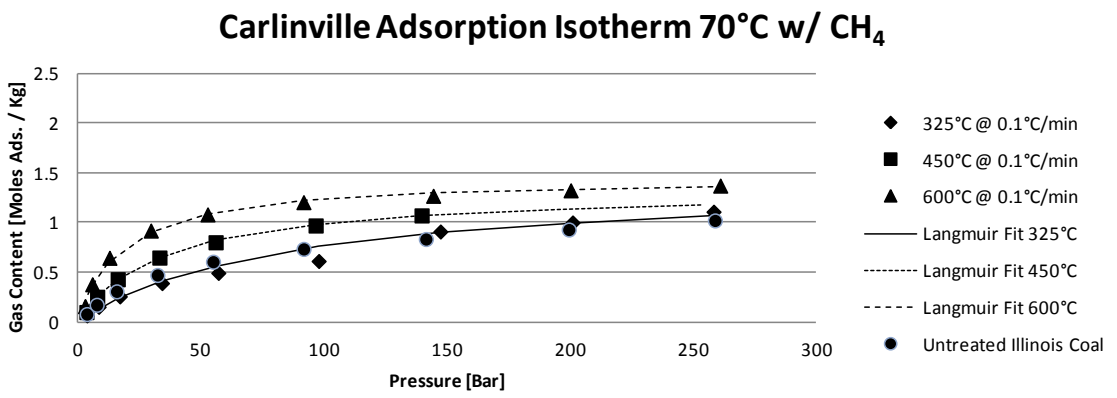


Figure D-1. Adsorption isotherms on untreated and thermally treated Carlinville coals treated with a heating rate of 0.1°C/minute. Isotherm measurements were performed with $CO_2$ and $CH_4$ at temperatures of 50 or 70°C.

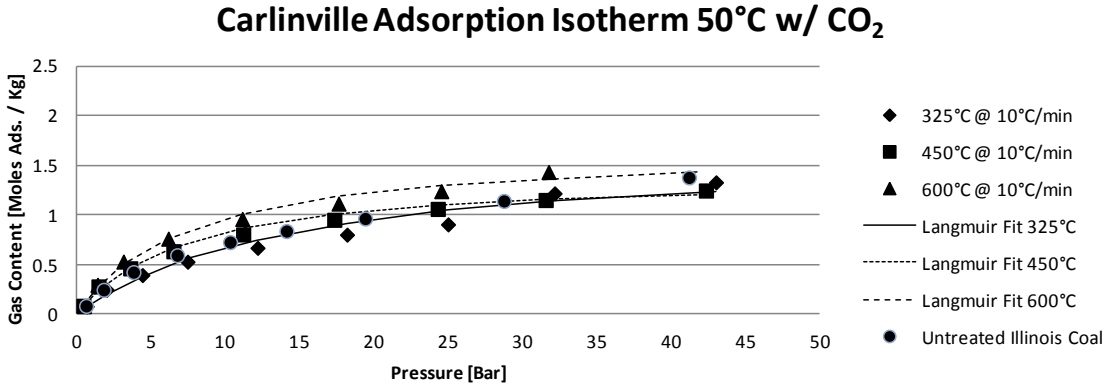


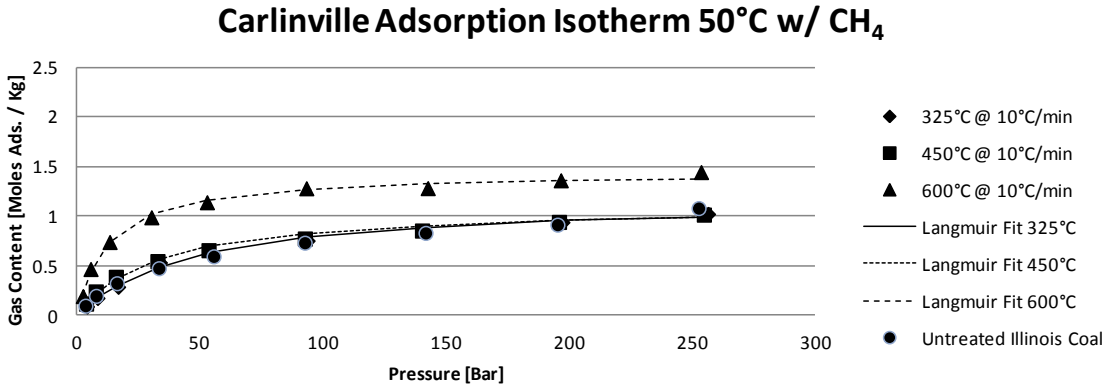

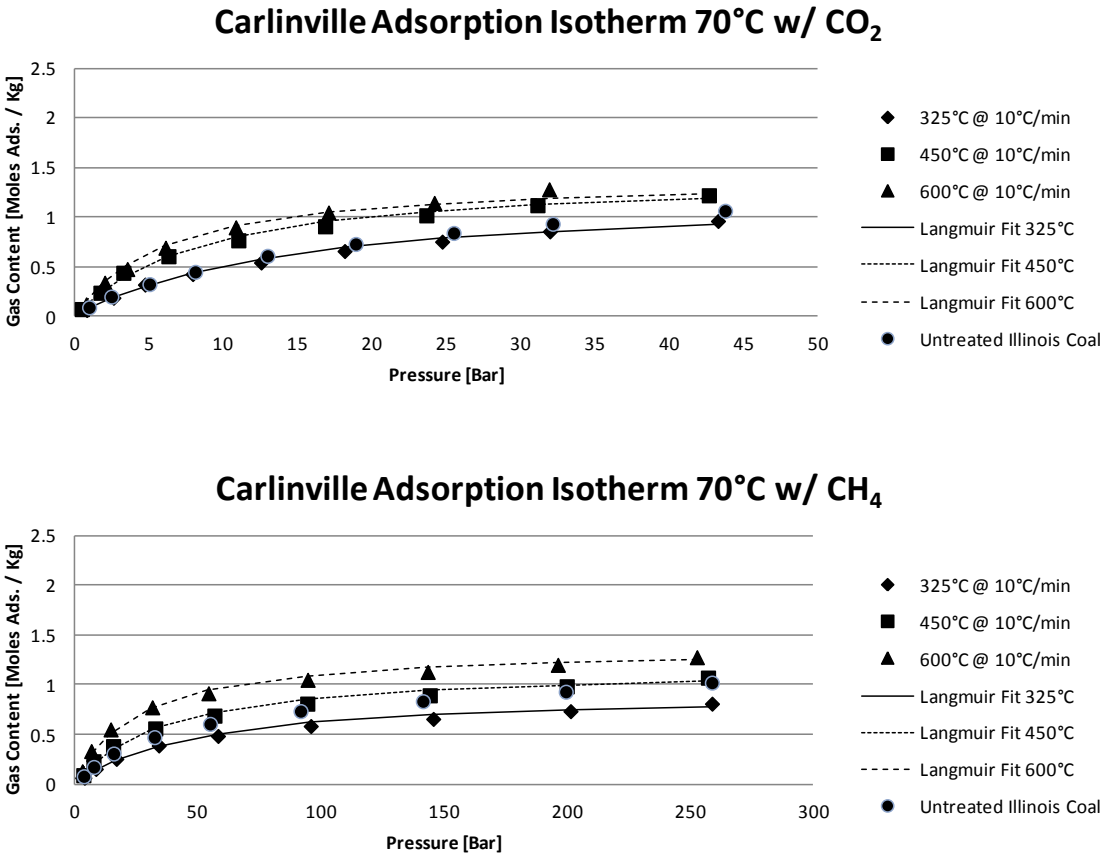


Figure D-2. Adsorption isotherms on untreated and thermally treated Carlinville coals treated with a heating rate of 10°C/minute. Isotherm measurements were performed with $CO_2$ and $CH_4$ at temperatures of 50 or 70°C.

Table D-1. Langmuir equation parameters for treated and untreated Carlinville coals. Units of V∞ are moles adsorbed per kilogram of coal. Units of β are 1/bar.

| ***Coal*** | *Langmuir Fit* | *$CH_4$ @ 50°C* | *$CH_4$ @ 70°C* | *$CO_2$ @ 50°C* | *$CO_2$ @ 70°C* |
|---|---|---|---|---|---|
| Carlinville | V∞ | 1.059 | 1.396 | 1.684 | 1.742 |
| | β | 2.717E-02 | 2.133E-02 | 8.224E-02 | 6.396E-02 |
| 325@0.1 | V∞ | 0.923 | 1.404 | 1.218 | 1.712 |
| | β | 3.159E-02 | 1.195E-02 | 1.054E-01 | 3.786E-02 |
| 450@0.1 | V∞ | 1.274 | 1.332 | 1.704 | 2.086 |
| | β | 4.343E-02 | 2.863E-02 | 1.293E-01 | 6.560E-02 |
| 600@0.1 | V∞ | 1.252 | 1.451 | 1.548 | 2.199 |
| | β | 7.123E-02 | 5.634E-02 | 1.867E-01 | 1.304E-01 |

| ***Coal*** | *Langmuir Fit* | *$CH_4$ @ 50°C* | *$CH_4$ @ 70°C* | *$CO_2$ @ 50°C* | *$CO_2$ @ 70°C* |
|---|---|---|---|---|---|
| Carlinville | V∞ | 1.059 | 1.396 | 1.684 | 1.742 |
| | β | 2.717E-02 | 2.133E-02 | 8.224E-02 | 6.396E-02 |
| 325@10 | V∞ | 1.180 | 0.921 | 1.676 | 1.254 |
| | β | 2.090E-02 | 2.104E-02 | 6.595E-02 | 6.721E-02 |
| 450@10 | V∞ | 1.106 | 1.180 | 1.417 | 1.424 |
| | β | 3.102E-02 | 2.734E-02 | 1.381E-01 | 1.196E-01 |
| 600@10 | V∞ | 1.441 | 1.364 | 1.687 | 1.420 |
| | β | 7.936E-02 | 4.143E-02 | 1.323E-01 | 1.632E-01 |

## APPENDIX E. NORTH ANTELOPE ADSORPTION ISOTHERMS

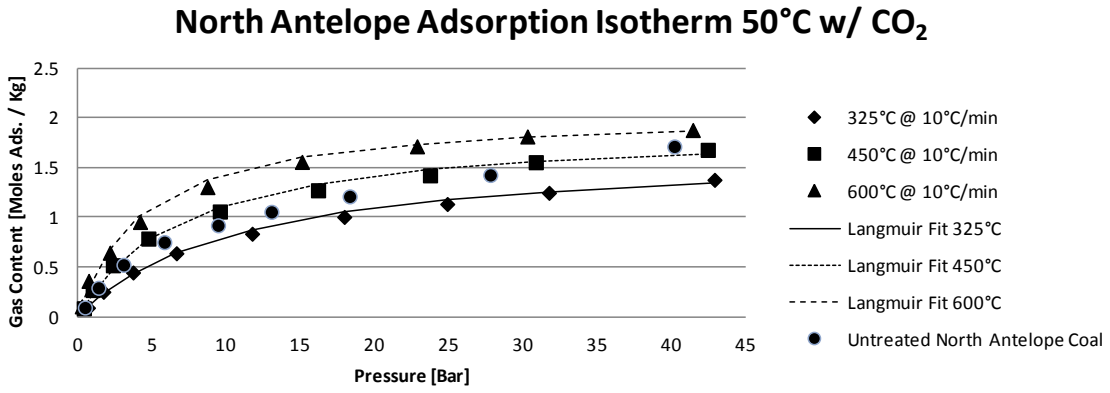


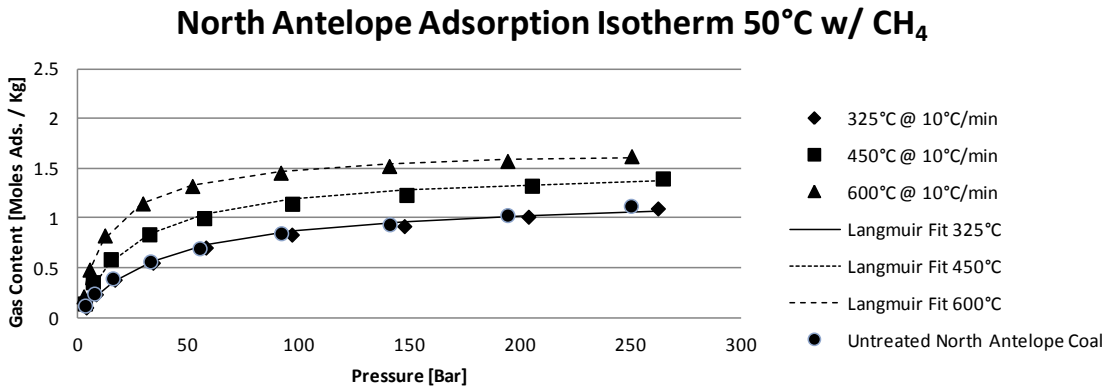


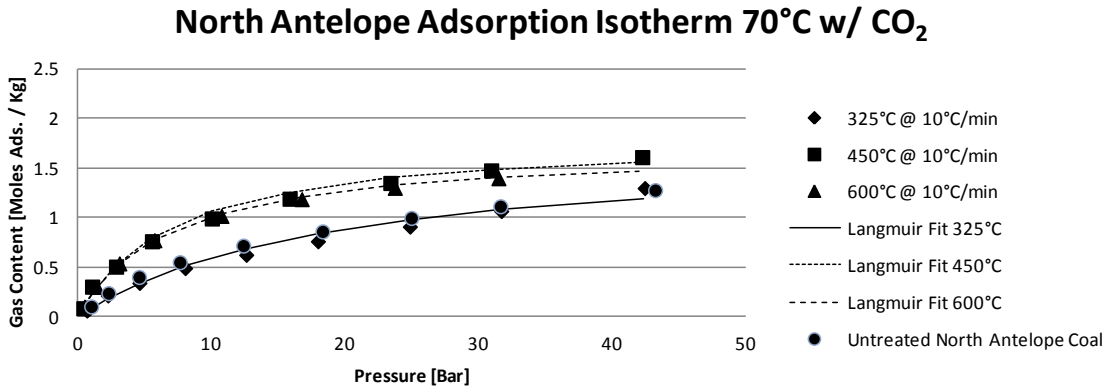

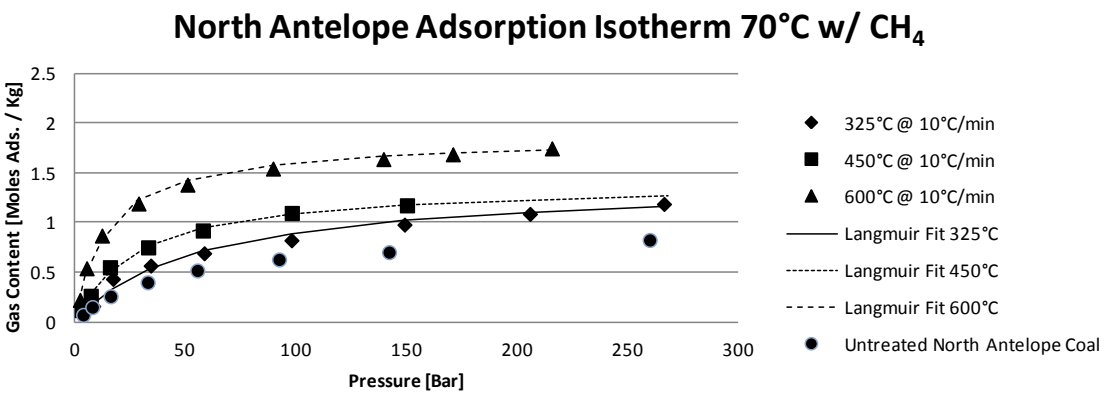


Figure E-1. Adsorption isotherms on untreated and thermally treated North Antelope coals treated with a heating rate of 10°C/minute. Isotherm measurements were performed with $CO_2$ and $CH_4$ at temperatures of 50 or 70°C.

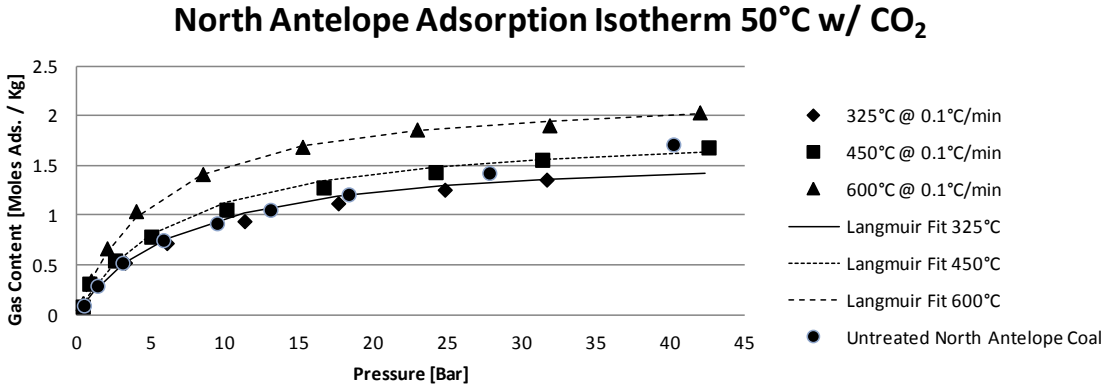


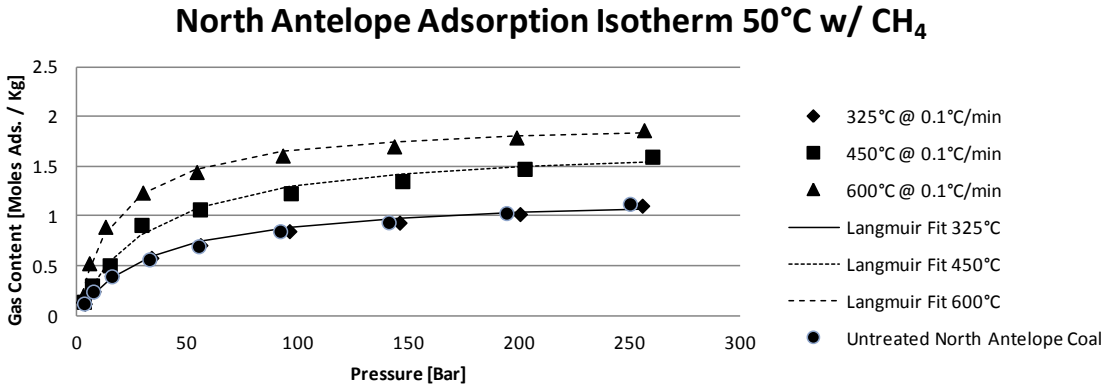

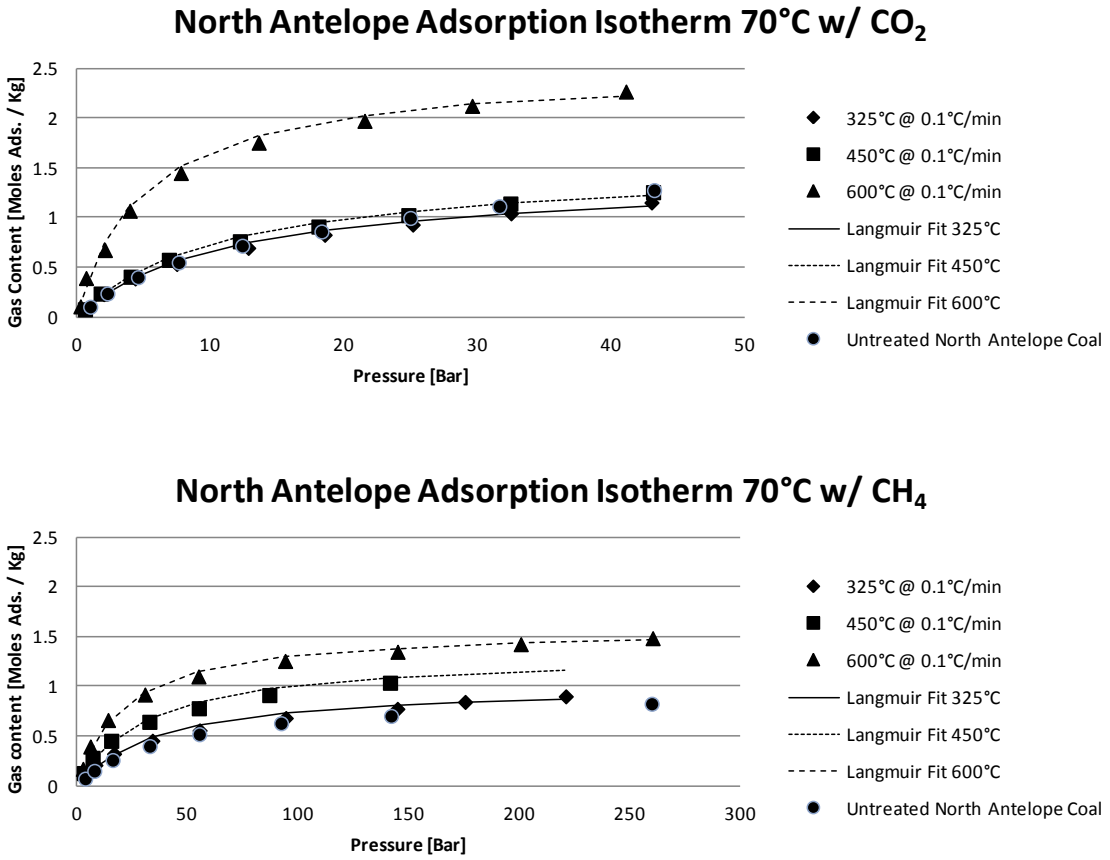


Figure E-2. Adsorption isotherms on untreated and thermally treated North Antelope coals treated with a heating rate of 0.1°C/minute. Isotherm measurements were performed with $CO_2$ and $CH_4$ at temperatures of 50 or 70°C.

Table E-1. Langmuir equation parameters for treated and untreated North Antelope coals. Units of V∞ are moles adsorbed per kilogram of coal. Units of β are 1/bar.

| ***Coal*** | *Langmuir Fit* | *$CH_4$ @ 50°C* | *$CH_4$ @ 70°C* | *$CO_2$ @ 50°C* | *$CO_2$ @ 70°C* |
|---|---|---|---|---|---|
| North Antelope | V∞ | 1.230 | 0.872 | 1.528 | 1.377 |
| | β | 2.867E-02 | 2.617E-02 | 1.683E-01 | 8.970E-02 |
| 325@0.1 | V∞ | 1.207 | 1.017 | 1.668 | 1.393 |
| | β | 2.937E-02 | 2.635E-02 | 1.403E-01 | 9.035E-02 |
| 450@0.1 | V∞ | 1.746 | 1.317 | 1.893 | 1.530 |
| | β | 2.957E-02 | 3.195E-02 | 1.497E-01 | 9.074E-02 |
| 600@0.1 | V∞ | 1.966 | 1.578 | 2.262 | 2.490 |
| | β | 5.516E-02 | 4.804E-02 | 1.954E-01 | 2.030E-01 |

| ***Coal*** | *Langmuir Fit* | *$CH_4$ @ 50°C* | *$CH_4$ @ 70°C* | *$CO_2$ @ 50°C* | *$CO_2$ @ 70°C* |
|---|---|---|---|---|---|
| North Antelope | V∞ | 1.230 | 0.872 | 1.528 | 1.377 |
| | β | 2.867E-02 | 2.617E-02 | 1.683E-01 | 8.970E-02 |
| 325@10 | V∞ | 1.221 | 1.392 | 1.677 | 1.732 |
| | β | 2.556E-02 | 1.802E-02 | 9.295E-02 | 5.229E-02 |
| 450@10 | V∞ | 1.501 | 1.392 | 1.906 | 1.833 |
| | β | 3.874E-02 | 3.618E-02 | 1.445E-01 | 1.365E-01 |
| 600@10 | V∞ | 1.698 | 1.836 | 2.057 | 1.696 |
| | β | 7.130E-02 | 6.900E-02 | 2.329E-01 | 1.484E-01 |